All Theses and Dissertations

2017-04-01

Strut-and-Tie Modeling of Multistory, Partially-Grouted, Concrete Masonry Shear Walls with Openings

Jeffrey Ryan Buxton
Brigham Young University

Strut-and-Tie Modeling of Multistory, Partially-

Grouted, Concrete Masonry Shear

Walls with Openings

Jeffrey Ryan Buxton

A thesis submitted to the faculty of
Brigham Young University
in partial fulfillment of the requirements for the degree of

Master of Science

Fernando S. Fonseca, Chair
Richard Balling
Paul Richards

Department of Civil and Environmental Engineering

Brigham Young University

ABSTRACT

Strut-and-Tie Modeling of Multistory, Partially-
Grouted, Concrete Masonry Shear
Walls with Openings

Jeffrey Ryan Buxton
Department of Civil and Environmental Engineering, BYU
Master of Science

Construction practices are constantly evolving in order to adapt to physical locations and economic conditions. These adaptations may result in more cost-effective designs, but may also come at a cost of strength. In masonry shear walls, it is becoming more common to reduce the amount of grouting from every cell to only those with reinforcement, a practice known as partial-grouting. Partially-grouted masonry responds differently and in a more complex matter to lateral loads as compared to fully-grouted masonry. The response is made even more complex by wall discontinuities in the form of openings. The main objective of this study is to validate the strut-and-tie procedure for the in-plane lateral strength prediction of partially-grouted, multistory, reinforced concrete masonry walls with openings.

The research included testing six three story, half-scale masonry shear walls. Half of the walls had door openings while the other half had window openings. The configurations were selected to represent typical walls in multi-story buildings. The measured lateral strength was compared to estimations from the equations in the US masonry code and to those from an equivalent truss model and a strut-and-tie model. The results show that the U.S. masonry code equations over predicts while the equivalent truss model under predicts the lateral strength of the walls. The results further show that the strut-and-tie model is the most accurate method for lateral strength prediction and is able to account for wall openings and partial-grouting.

ACKNOWLEDGEMENTS

I would like to thank Dr. Fernando Fonseca for his continual support and encouragement especially as I met numerous roadblocks along the way. I would also like to thank him for hiring me to do research for him starting in my last year of my undergraduate studies. His enthusiasm for all things structural was a major aspect in my decision to pursue a master's degree at Brigham Young University. I would also like to thank Dr. Henry Christiansen and any others whose donations funded my tuition and allowed me to focus on my studies and research including those locally and the Canada Masonry Design Centre. I would like to give a special thanks to Ernesto Fortes who allowed me to work on his project and trusted me to work on other projects in his doctoral dissertation. I would also like to thank those who helped for their assistance in the lab: Dave Anderson, Lab Manager; Rodney Mayo, assistant lab manager; David Ochoa, Kyle Chavez, Rawley Selk, and Clay Hansen, undergraduate lab technicians; and Aaron Roper, Theodore Moffett, and Ryan Beaumont, undergraduate lab assistants.

Lastly, I would like to thank my friends and family who have supported me in my education. I am grateful to my parents for supporting me not only financially, but also for allowing me to intern in Arizona and Texas. I would like to also thank my fiancé, Emily Hall, for supporting me in the last bit of my education and encouraging me to finish my education.

TABLE OF CONTENTS

LIST OF TABLES

LIST OF FIGURES

1 INTRODUCTION

1.1 Background

Concrete masonry is a modular construction method consisting of the assembly of concrete masonry units (CMUs), mortar, grout, and reinforcing steel rebar for reinforced masonry. Typically, CMUs are placed on a bed of mortar that forms a horizontal joint between the masonry units; mortar is also placed along the vertical joint between the units. In the case of reinforced masonry, steel reinforcement is placed in the hollow cells of the CMUs at various locations, either vertically or horizontally, to provide resistance to tensile forces. The hollow cells of the CMUs may or may not be grouted while hollow cells containing reinforcement are always grouted, which creates in essence a unified system. When the entire system is grouted, the construction is called *fully-grouted* and when only a few cells of the system are grouted, the construction is called *partially-grouted*.

Concrete masonry is used in many types of buildings throughout the world and is designed to resist a variety of loading conditions. In the United States and other parts of the world, concrete masonry walls are used as the lateral force resisting system of structures subjected to wind and/or seismic loads. While concrete masonry is used in the US predominately for warehouses and large retail buildings, it is used in many parts of the world for ordinary construction from residential to commercial buildings. Developing countries use concrete masonry for residential construction ranging from single-story homes to multistory buildings,

1

where concrete masonry wall may be slender and have door and window openings. These walls could be fully-grouted, but to reduce costs, could be partially-grouted.

The design principles for concrete masonry are similar to those of reinforced concrete, both for analytical and empirical design procedures. These design procedures continue to evolve as research is conducted and construction practices adapt to economic conditions and different locations. These design procedures are also adjusted to provide adequate strength in various situations such as during an earthquake. The seismic response of masonry shear walls has been studied considerably and partially-grouted shear walls continue to be studied due the complexity of the system and to understanding their response to different loading conditions.

Partially-grouting is a recent construction practice and is used to reduce costs and the structural weight of masonry walls while still providing an adequate shear resisting system. Because not every cell in the wall is grouted, i.e., the wall is not a solid system, the complexity of the system increases. The capacity and behavior of a partially-grouted wall depends largely upon the material properties of the individual components of the wall as well as the complex interaction between components. The analysis of this system would involve complex numerical methods, be time consuming, and increase the cost of the design—offsetting the savings in construction. Currently, the U.S. Masonry Standards Joint Committee code (MSJC) code simply penalizes the design of partially-grouted walls in order to account for the loss of strength. The code also does not prescribe a method to account for openings of various sizes in the wall.

1.2   Research Scope

The study presented herein is part of a comprehensive research program conducted to determine the capacity and behavior of multistory high-strength concrete masonry walls with

2

openings. For that purpose, several partially-grouted, multistory, half-scaled concrete masonry walls with openings were constructed and tested. A detailed description of the research program is given by Fortes (2017).

The objective of this thesis was to expand the strut-and-tie methodology to multistory, partially-grouted walls with openings The study is devoted to analyzing six of the walls tested: three walls with door openings and three walls with window openings. Emphasis is on the analysis of the walls rather than on the experimental program. Nonetheless, a brief overview of the construction, testing, and lateral strength results of the six walls is given.

The strut-and-tie methodology used in this study was introduced by Schlaich et al. (1987) for reinforced concrete structures. That methodology was adapted to concrete masonry structures by Dillon (2015), who studied fully- and partially-grouted masonry walls with and without openings—no wall in the used database, however, was more than one story high. The objective of this thesis was to expand the methodology developed by Dillon (2015) to multistory, partially-grouted walls with openings.

1.3   Thesis Outline

This thesis is organized into six chapters. The first chapter is this introduction and gives background information and scope of the research. The second chapter contains a literature review of past studies on fully- and partially-grouted masonry walls with and without openings. Chapter 3 briefly describes the construction and testing of the six walls and measured results. The fourth chapter describes various prediction methods for the lateral capacity of masonry walls culminating with the strut-and-tie procedure and computed results. Chapter 5 presents a comparison and discussion of the results along with a discussion of the effects of the different

3

parameters of the strut-and-tie model. The final chapter presents the conclusions of this study and provides recommendations for future research.

2   LITERATURE REVIEW

2.1   Fully-Grouted Shear Walls

Masonry walls under in-plane lateral loads can typically be modeled as cantilever beams using conventional beam theories. The governing principle of Timoshenko Beam Theory is that beams deflect according to their resistance to both flexure and shear. Flexure dominates the response of beams with large aspect (height to width) ratios while shear dominates the response of beams with small aspect ratios.

Boundary conditions also influence the response of masonry walls to lateral load. Haach et al. (2013) noted that in both cantilever and fixed-end shear walls, the compressive stress travels diagonally from the point of load application to the toe of the wall, as shown in Figure 2-1. The concentration of compressive stresses at the toe of the wall may cause crushing of the masonry at that location while tensile stresses, which are induced perpendicular to the diagonal compressive flow, may cause cracks along that diagonal. The authors also noted that cantilever walls are subject more to the effects of flexure than to the effects of shear and display flexure cracking on the trailing side (the side of load application) along the bed joints due to the flexural tensile stresses and the uplift of the wall. In contrast, fixed-end walls are subject more to the effects of shear and experience diagonal cracking, but can also exhibit flexural cracking.

5

The behavior of masonry shear walls is also affected by axial load and by the placement of vertical and/or horizontal reinforcement. Masonry shear walls experience three failure modes classified as:

1. Failure by flexure

    a. Flexural cracking

    b. Yielding of longitudinal reinforcement

    c. Crushing of Masonry

2. Failure by shear

    a. Diagonal cracking

    b. Yielding of transversal reinforcement

    c. Sliding

3. Mixed shear-flexure mode
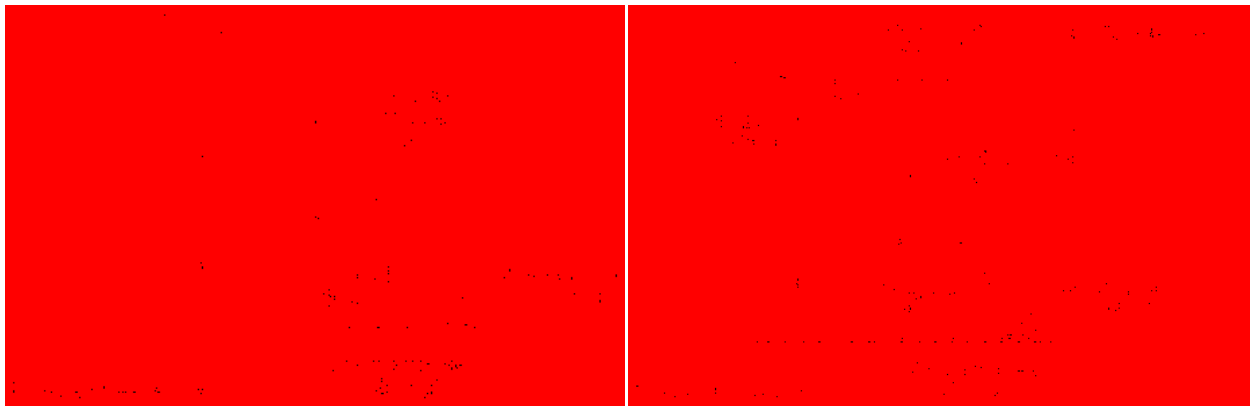
(a) Cantilever Walls   (b) Fixed End Walls

Figure 2-1: Possible Crack Patterns Caused by In-plane Horizontal Loading of Masonry Walls (Haach et al. 2013)

2.2   Partially-Grouted Shear Walls

Partial grouting can significantly alter the structural properties of masonry shear walls and should be accounted for in analysis methods. In the current MSJC (2013) code, a factor is used to penalize partial grouting. The factor reduces the predicted shear strength of a partially-grouted element by 25%. The current penalty method is a "Band-Aid" approach towards conservatism because available data related to partially-grouted walls is limited and it does not adequately account for the complex behavior of partially-grouted shear walls.

Several factors need to be investigated for a robust design equation for partially-grouted walls to be developed. The reinforcement (and corresponding grouting) spacing has been cited as a critical parameter affecting the behavior of partially-grouted walls and several studies have been conducted to determine the effects of varying the distributions of vertical and horizontal reinforcement (Voon and Ingham, 2006; Minaie, 2010; Nolph, 2010). Voon and Ingham (2006), for example, showed that evenly distributed shear reinforcement prevents catastrophic failure in both fully- and partially-grouted walls and enables the shear wall to act in a ductile matter. Such a behavior was because the stresses could be distributed over a greater area of the wall after initial shear cracking, which helped dissipate energy. The authors observed that when shear reinforcement was distributed throughout the wall, shear cracks were also distributed throughout the wall, which resulted in a more ductile failure.

2.3   Fully-Grouted Masonry Shear Walls with Openings

As mentioned previously, the capacity of masonry shear walls with large aspect ratios is usually governed by flexure. In a study to determine the behavior of multistory masonry walls, Leiva et al. (1990) tested several multistory walls. The specimens were designed to fail in

7

flexure. In the two-story, fully grouted specimens with door openings, the authors observed that because the wall piers were stronger than the lintels, cracks and hinges formed at the edges of the lintel and at the slab-wall interface as shown in Figure 2-2. The observations during the testing aligned well with the predicted failure mode shown in Figure 2-3 (Klingner and Leiva 1992).
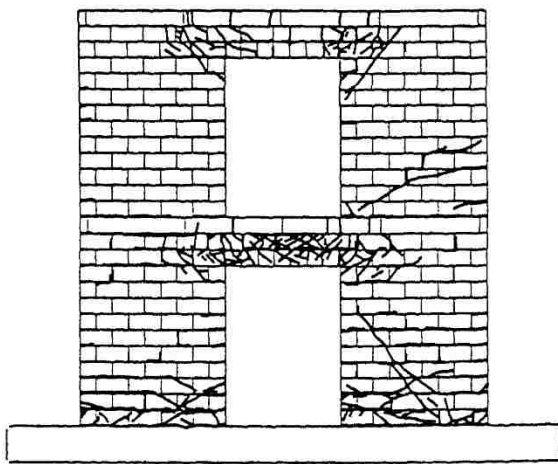
Figure 2-2: Two-Story, Fully Grouted Wall Crack Pattern (Klingner and Leiva 1992)
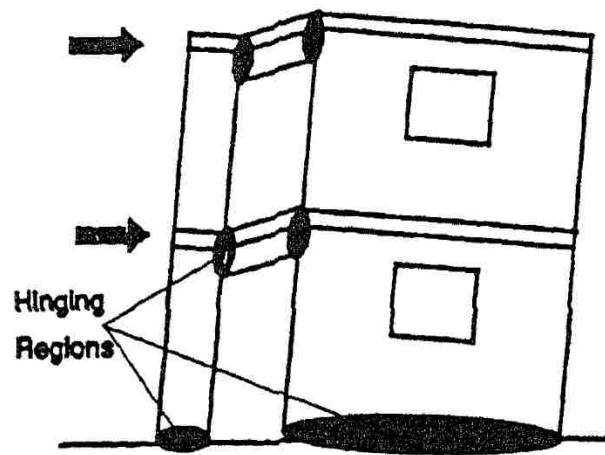
Figure 2-3: Coupled Wall-type Collapse Mechanism (Klingner and Leiva 1992)

2.4 Partially-Grouted Masonry Shear Walls with Openings

Voon and Ingham (2008) investigated the strength reduction of partially-grouted masonry walls with openings. Eight walls were tested with windows and doors of different sizes including walls with two openings. The authors observed that none of the walls exhibited a sudden failure because a grouted bond beam was located at the top of the walls. The bond beam caused a frame-type action at latter stages of testing. The testing results confirmed that strength reductions occur with masonry walls with openings and that when openings become taller, the strength decreases due to the steepened diagonal strut that forms behind the opening. The results also showed that the double bending behavior of central piers in walls with two openings significantly increased the wall strength.

8

2.5 Strut-and-Tie

Strut-and-Tie models evolved from the truss model that was developed in the early 20th century. Although parts of the strut-and-tie model existed for some time, Schlaich et al. (1987) developed a consistent design procedure for structural concrete structures using strut-and-tie models. The authors theorized that concrete structures could be divided into "B" and "D" regions (B for Bernoulli and D for discontinuity, disturbance or detail). B regions could be designed using Bernoulli Theory, but D regions could not because they contain areas where the strain distribution is significantly nonlinear, e.g., near concentrated loads, comers, bends, openings and other discontinuities. In order to design these D regions, a different approach should be used and the authors developed a strut-and-tie methodology to design these regions.

Schlaich et al. (1987) were the first researchers to detail specific principles for developing strut-and-tie models for concrete structures. These models can be used to determine the placement of reinforcing steel, but the principles can also be used for analysis. Within a reinforced concrete structure, modeling is performed by identifying compressive and tensile elements. Struts are zones of compression while ties are zones of tension. The location of these elements can be determined based on load paths, but are up to the discretion of the engineer. Within reinforced concrete structures, struts are typically the cementitious material, which perform well under compression, while the ties are the reinforcing steel. These elements intersect at nodes, and eventually the strut and ties transfer the force to supports or other boundary conditions.

2.5.1 American Concrete Institute (ACI) code 318-11

ACI code 318-11 Appendix A (2011) contains the general process originally conceived by Schlaich et al. (1987). The strut-and-tie analysis is a strength design procedure whereby struts and ties are laid out in an idealized truss scheme that is capable of transferring all factored loads to the supports or adjacent B-regions. The model must be in equilibrium and even though the model can be represented as an idealized truss, the dimensions of the struts, ties, and nodes are considered, i.e., each element has a sufficient cross-section to resist the applied load. A simple strut-and-tie model representing a deep beam is shown in Figure 2-4. Ties are permitted to cross struts and other ties, but struts can only cross or overlap another element at nodes. The strength of ties is its cross sectional area multiplied by its tensile strength. The strength of struts, however, is based on the minimum of the compressive strength of the strut or connecting nodes.
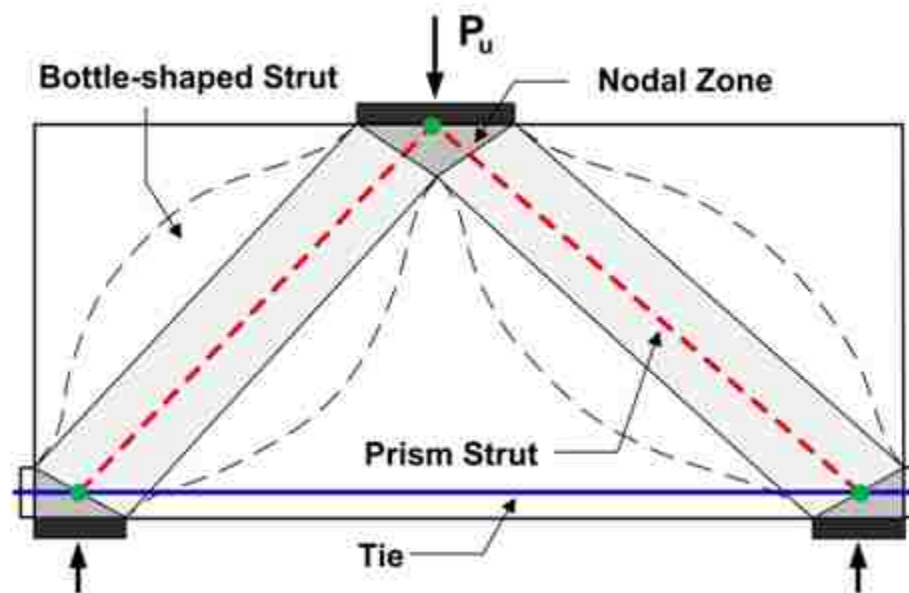
Figure 2-4: Simple Strut-and-Tie Model

2.5.2   Strut-and-Tie Variations

Voon and Ingham (2008) applied classic strut-and-tie principles to the analysis of ten walls with various openings. The authors adjusted the strut-and-tie procedure by applying the load in the middle of the wall rather than on the edge. The method allowed the authors to better predict the strength of certain wall configurations. However, the procedure used was more like an equivalent truss model than a strut-and-ties model because the width of the strut was not considered and other classic strut-and-tie modeling procedures were neglected.

Nolph (2010) and Elmapruk (2010) each tested six partially-grouted masonry walls. They compared the measured results to those obtained using the MSJC shear equation and to those from a strut-and-tie model. The method the authors used for determining the width of the struts was unconventional since it relied only upon the depth of the bond beam on top of each specimen. The method simplified the calculations but neglected the nodal strength contribution from ties, which is a key component of the strut-and-tie methodology.

Dillon (2015) conducted a comprehensive analysis using the strut-and-tie modeling procedure to calculate the lateral strength of several masonry walls. The author adapted the ACI 318 reinforced concrete procedure to masonry structures. The modifications included changing the stress block modifier from 0.85 to 0.8 to better align with conventional masonry design. The author also introduced the concepts of toe extension, coupling beam, and strut inclination factor in order to adjust the strut-and-tie procedure to accommodate partially grouted walls. The study showed the effectiveness of strut-and-ties in modeling all masonry configurations including partially-grouted walls with and without openings.

11

3 EXPERIMENTAL TEST SPECIMENS

3.1 Introduction

Six half-scaled specimens were constructed by a mason for this study; three specimens had door openings and three specimens had window openings. Each specimen had the same overall dimensions. The specimens were tested under a quasi-static load until failure. A brief description of these six walls and the results of the tests are given in this chapter. A comprehensive description of the overall testing program is given by Fortes (2017).

3.2 Wall Specimens

The test specimens in this study come from a more comprehensive study on multistory, partially grouted walls with openings. Six of the walls used for that study are used within this study. This includes the walls that have door and window openings and excludes those with a reinforced concrete T-beam. The designs of the walls with doors are shown in Figure 3-1. The design for the first two walls with windows (Walls 4 and 7) is shown in Figure 3-2 and the design for the third wall with windows (Wall 10) is shown in Figure 3-3. The difference in design between Walls 4 and 7 and Wall 10 is that the fifth course reinforcement in Walls 4 and 7 only spans the width of the window opening while Wall 10 has reinforcement spanning the entire length of the wall.
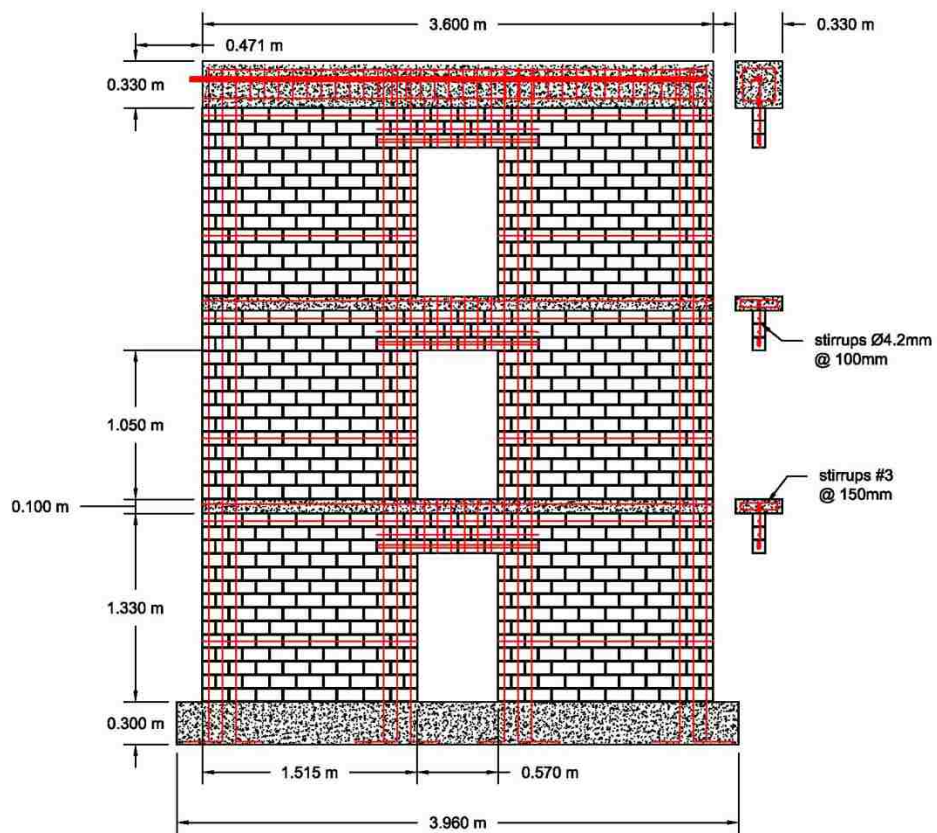
Figure 3-1: Geometry and Reinforcement Details of Walls with Door Openings
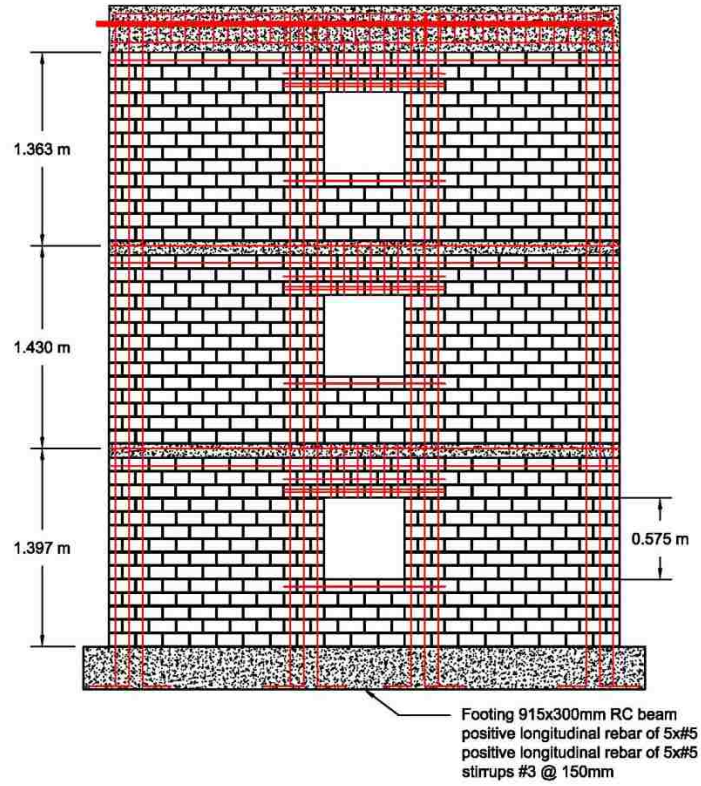
Figure 3-2: Geometry and Reinforcement Details Wall 4 and Wall 7.
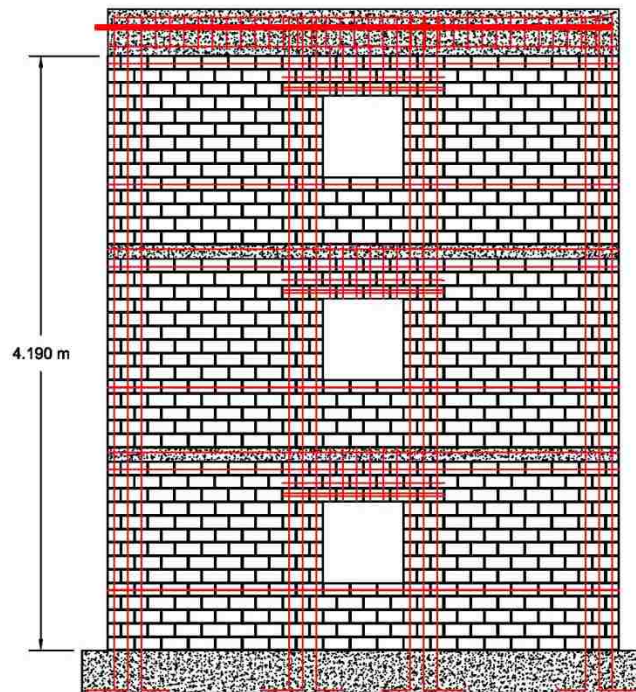
Figure 3-3: Geometry and Reinforcement Details of Wall 10

The masonry walls were constructed on top of a reinforced concrete footing. The footing dimensions were 4 ft. x 13 ft. x 1 ft. A reinforcement cage was constructed of five #5 longitudinal bars on top and bottom and #3 stirrups. The vertical bars for the first story of the walls were fastened to the footing reinforcement cage at the appropriate locations. Each of these vertical bars included a 90-degree bend to prevent pullout. PVC pipe was placed every 3 ft. in the footing order to provide means to secure the foundation to the laboratory floor using dywidag bars. Four U-shaped bars were placed in the footing as pick points to provide means for the entire wall to be transported to the testing place. The nominal concrete strength for the footing was 4000 psi (28 MPa) and was poured into the footings with a slump of approximately 7 inches. The concrete was consolidated using a vibrator.

A mason and graduate assistants constructed the walls in a running bond using 4 in x 4 in x 8 in concrete masonry units (CMU) with face shell bedding. The CMUs were a half-sized model of 8 in x 8 in x 16 in CMU. This was required because of construction restraints to build a three story wall within the laboratory, which itself is only two-stories high. The walls were approximately 142 in (3.6 m) long, 177 in (4.5 m) tall, and 3.55 in (90 mm) wide. The door openings were 41 in (105 mm) tall and 22 in (57 mm) wide. The window openings were 23 in (58 mm) tall and 22 in (57 mm) wide. Only cells with reinforcing steel were grouted. Reinforcement consisted of #3 for all locations except for the top concrete beam and the stirrups which were #4 and 0.165 in. diameter (4.2 mm), respectively.

The walls were designed such that they were taller than they are wide with an aspect ratio of 1.25. This was done in an attempt to increase the effect the openings have on the lateral strength of multistory walls with openings. If the aspect ratio were relatively small (<<1) and the

openings were small compared to the size of the wall, the effect of openings could be neglected. This design parameter was coupled with partial grouting in a multistory configuration (three stories in this study).

Jamb reinforcement was used in conjunction with partial grouting. In other words, vertical reinforcement was only placed on the edges of the walls and borders of the openings. Horizontal reinforcement was placed in the course of masonry directly beneath the floor slab for the bond beam as well as in the lintel above the openings. In the walls with doors, additional horizontal reinforcement was placed in the fifth course of masonry in each story spanning the width of the pier. In the walls with windows, horizontal reinforcement was placed directly underneath the window. As mentioned previously, the horizontal reinforcement extended just beyond the window opening in Walls 4 and 7 while in Wall 10, this reinforcement extended across the entire wall. Stirrups were used in the floor and roof slabs and lintels.

3.3 Equipment and Facilities

The walls were built in sets of three walls, meaning that three footings were poured and the walls built on top of them as shown in Figure 3-4. The walls were constructed with the help of two tripods. Scaffolding was used to help construct the second and third stories as shown in Figure 3-5. Walls were cured for three weeks prior to transporting them into the testing area except for Wall 1, which cured for four weeks. The original plan was to have every wall cure for four weeks, but due to time constraints, the curing time was reduced to three weeks. After testing, the walls were dismantled and disposed. As the third wall of the set was completed, the footings for the next set were constructed.

16

Figure 3-4: Footing Reinforcement Cages and Forms
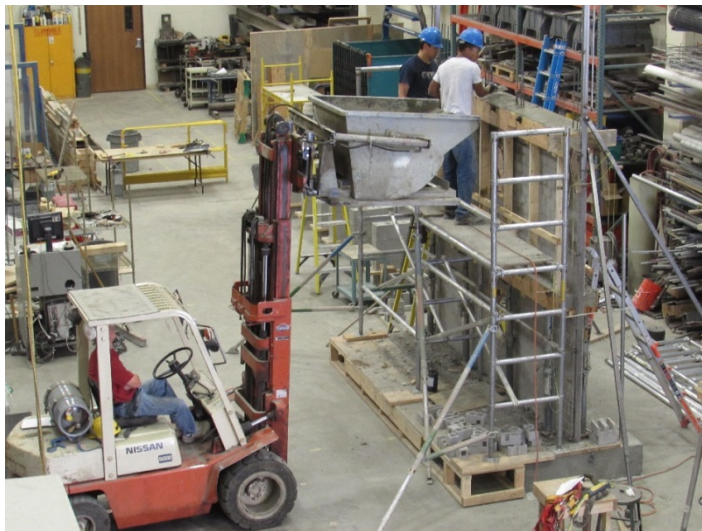
Figure 3-5: Construction of the Walls and Pouring of the Second Story Slab Showing the Scaffolding and Tripods

3.4   Test Procedure

Walls were tested in a custom apparatus that allowed a MTS actuator to apply a cyclical, incremental, displacement-controlled load to the wall as shown in Figure 3-6. Every wall was lifted and placed into hydrated gypsum that when hardened would reduce stress concentrations on the base and provide a level testing surface. Walls were secured to the lab floor using dywidag bars. The walls were prevented from displacing out of plane and from complete collapse by a system of supports shown in Figure 3-7. The system allowed for movement in the direction of loading and was checked before each wall test to make sure that the system did not restrain the movement of the wall, which would artificially increase its strength.

Figure 3-6: Wall Testing Apparatus

Figure 3-7: Out-of-Plane Bracing System

The walls were instrumented with LVDTs, string pots, and strain gauges as shown in Figure 3-8. LVDTs and string pots measured the displacement of critical joints such as those between the interfaces of the concrete slab and wall, the wall openings, and the joints above and below openings as illustrated in Figure 3-9. String pots were also used to measure the displacement of the wall laterally and the deformation of the wall face. Strain gauges were also installed at critical locations of the reinforcing steel as shown in Figure 3-10.

Prior to testing, a load of 11.43 kips (50.8 kN) was placed on top of the wall. The load consisted of very heavy steel sections as shown in Figure 3-6. A layer of neoprene padding was placed under the load to prevent stress concentrations. A complete test lasted between three and four hours with data recorded throughout the test. The walls were tested using a displacement controlled protocol. Figure 3-11 shows the loading protocol and the actual load applied through

19

Figure 3-8: Wall Instrumentation

T LVDT I String Pot
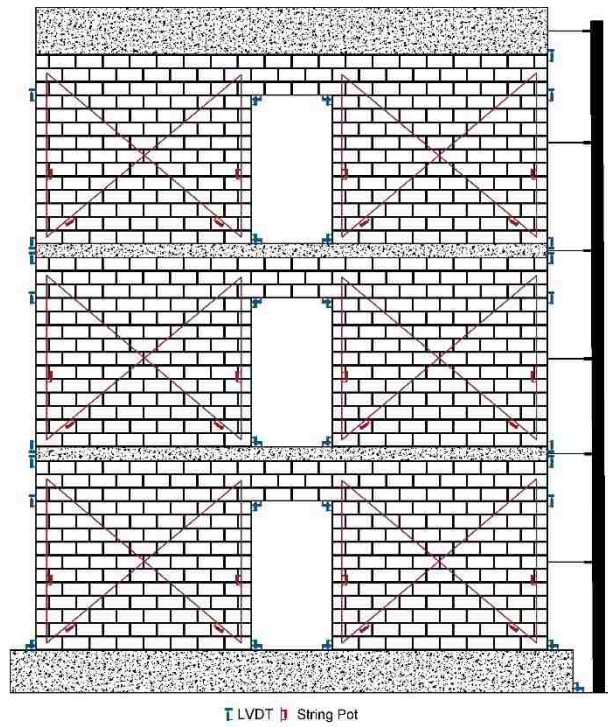
Figure 3-9: LVDT and String Pot Layout

time for one of the walls tested. The pause shown in the loading protocol was to allow time for documentation of the cracks that formed after each displacement cycle. After each push or pull of the actuator, cracks were documented with markers to track their propagation as shown in Figure 3-12.
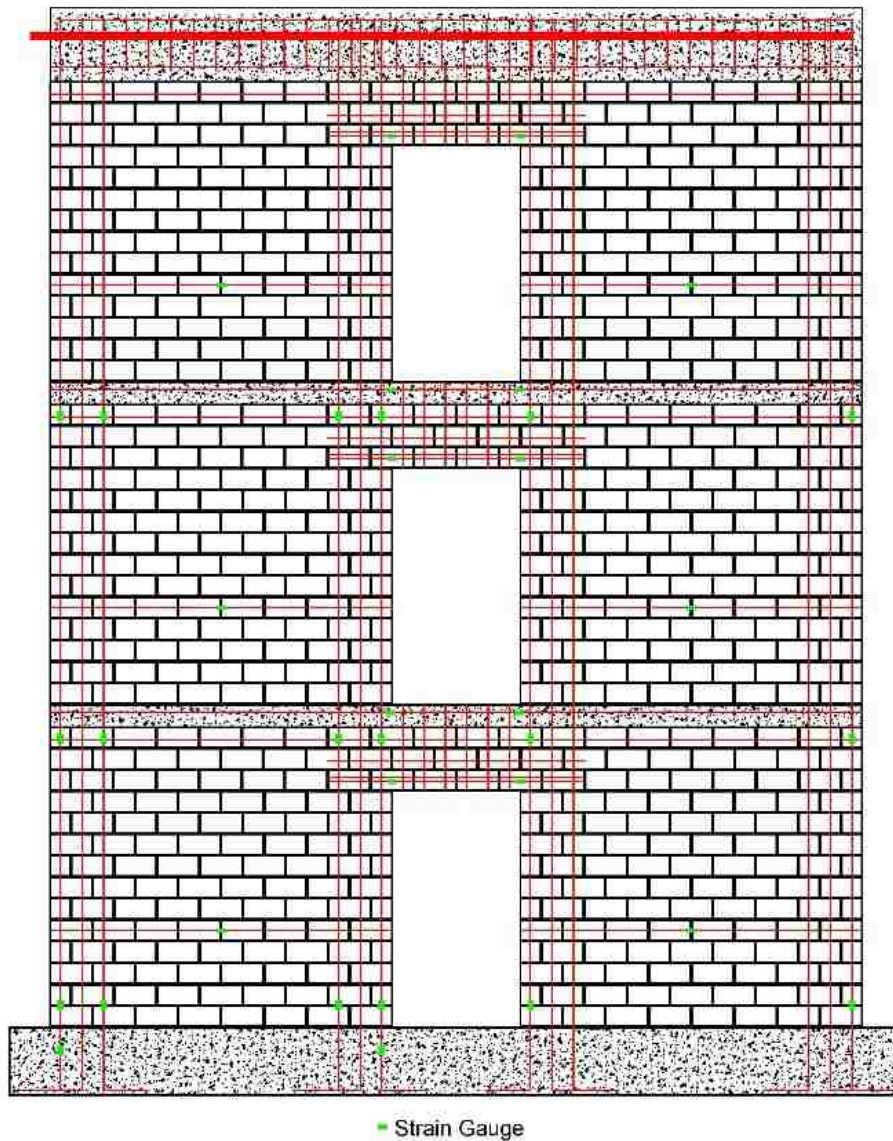
▪ Strain Gauge

Figure 3-10: Strain Gauge Layout

21
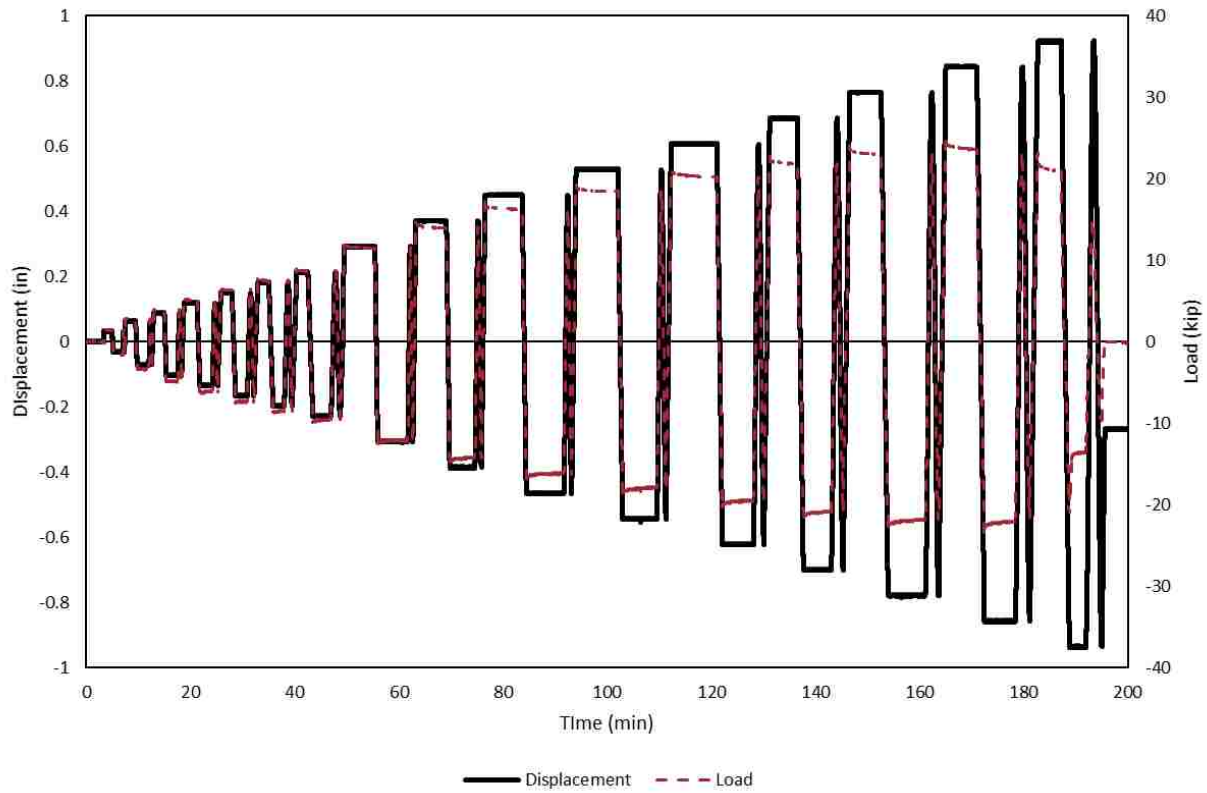
Figure 3-11: Actuator Displacement and Load Through Time for Wall 10.

Figure 3-12: Marking Cracks During Testing

22

3.5 Experimental Results

The test of each wall was successful and adequate data were obtained for each case. Table 3-1 shows the measured maximum lateral load of each and the corresponding deflection at that load. For the six walls related to this thesis, the average lateral strength was 23.7 kips (106 kN) with a standard deviation of 1.73 kips (8 kN) and an average deflection at the top of the wall of 0.59 inches (15 mm) at that strength. Loading envelopes for walls with doors and windows are shown in Figure 3-13 and Figure 3-14, respectively. The load-displacement curves for each wall are provided in Appendix A. In general, all of the walls followed a similar response in the linear regime and in early parts of the nonlinear regime. In the later parts of the nonlinear regime, the walls differed in their response. Of particular note, it can be readily seen that Wall 7 was more ductile than the other walls with door openings. This is most likely as a result of the stirrups in the fifth course being hooked around the vertical bar as opposed to the other two walls having simply a straight bar with no hooks at their ends. Additionally, Wall 10 was more ductile and had higher strength than the other walls with window openings. The increase in strength and ductility can be attributed to the difference in the reinforcing steel in the fifth course of masonry in each story. As aforementioned, the reinforcing steel in Wall 10 extended the entire length of the wall as compared to Walls 4 and 7 where the steel was only the width of the opening.

Each wall failed in a similar manner. As the walls were being tested and crack propagations were recorded, the largest and most substantial cracks always occurred in the first story. Nonetheless, a wall occasionally failed in the second story. Each wall developed a cracking pattern similar to one shown in Figure 3-15. Cracks marked in black are from when the wall is pushed and those in red are from when the wall is pulled. In all cases, the failure was by shear. Haach et al. (2013) mentioned that walls in a fixed-end configuration (double curvature)

are more likely to exhibit diagonal shear failures characterized by a diagonal crack propagating

through the wall.

Table 3-1: Lateral Strength and Deflection of Wall Specimens

Wall	Opening Type	Strength		Deflection	
		(kips)	(kN)	(in)	(mm)
1	Door	26.5	118	0.57	14
4	Window	22.8	101	0.45	11
5	Door	21.9	97	0.62	16
7	Window	22.5	100	0.48	12
8	Door	23.9	106	0.85	21
10	Window	24.8	110	0.55	14
Average		23.7	106	0.59	15
Standard Deviation		1.73	8	0.14	4
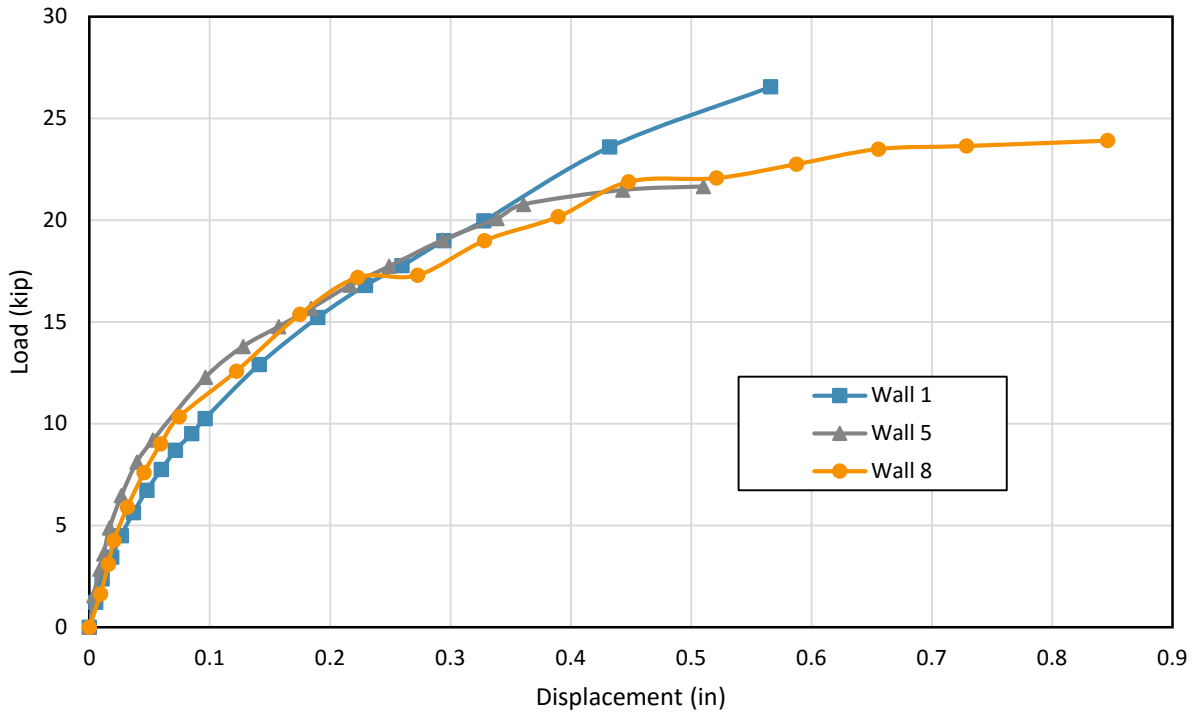
Figure 3-13: Loading Envelope for Walls with Door Openings
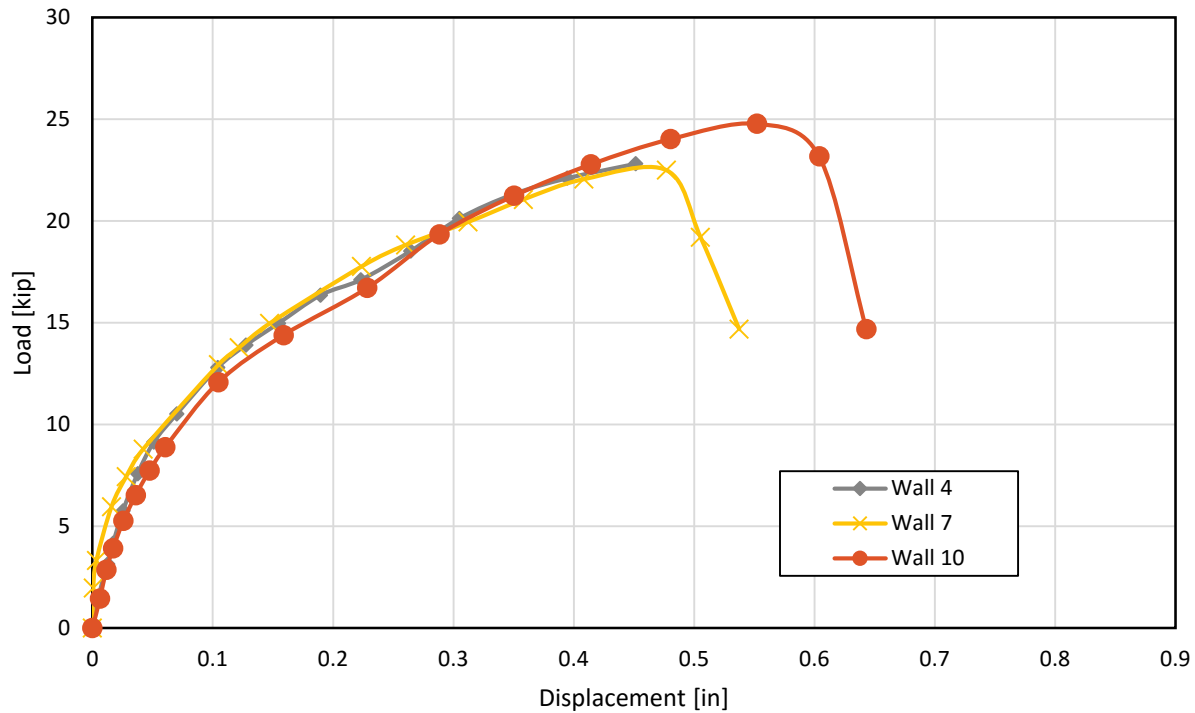
Figure 3-14: Loading Envelope for Walls with Window Openings

Cracks first appeared in the first story in the ungrouted area along the critical failure plane in each direction. Soon cracks would appear parallel to the first crack in the upper two stories, but to a lesser degree as shown in Figure 3-16 and Figure 3-17. In the early parts of the tests, cracks parallel to the initial crack would form in the ungrouted section. This pattern continued until the later stages of the tests when the vertical reinforcement would yield and cracking was observed through the grouted sections, as shown in Figure 3-18. The cracking pattern observed is similar to those described in other studies (Voon and Ingram, 2006; Nolph, 2010; Elmapruk, 2010), except these studies only involved one-story specimens as shown in Figure 3-19 and Figure 3-20, respectively.
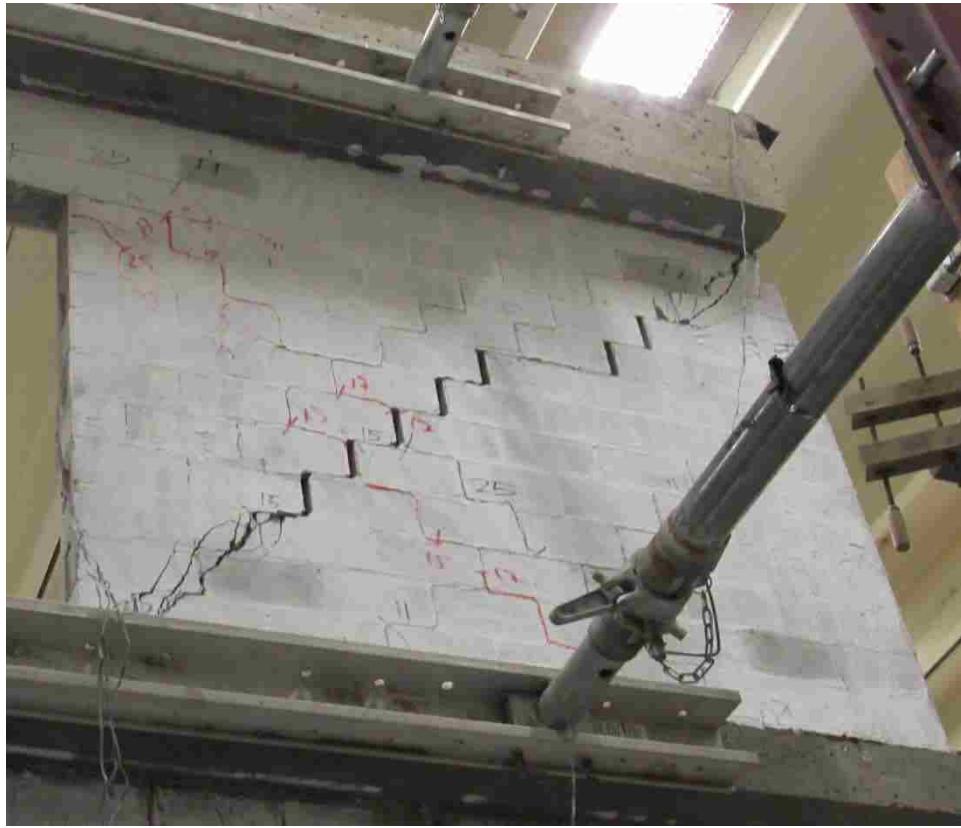
Figure 3-15: Shear Cracking
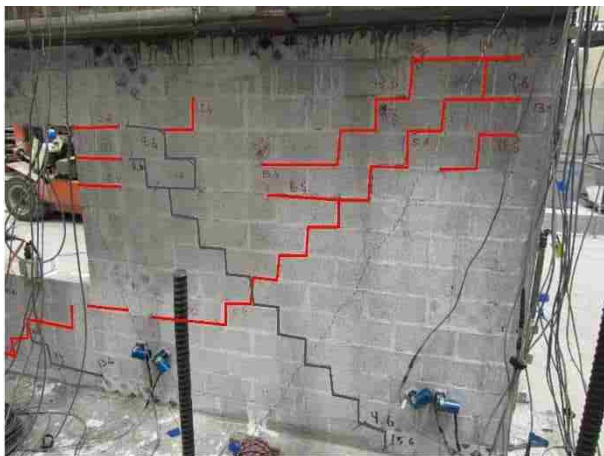
Figure 3-16: First Story Cracking Pattern
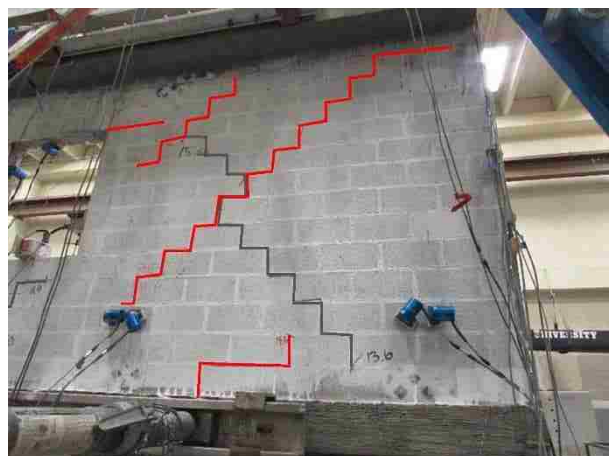
Figure 3-17: Third Story Cracking Pattern

Figure 3-18: Cracking Through the Grouted Cells

Figure 3-19: Voon and Ingham (2006) Wall Cracking Patterns
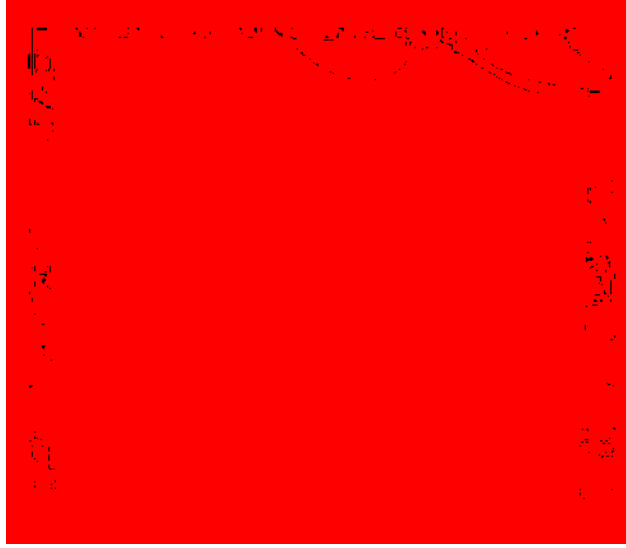
Figure 3-20: Nolph (2010) Wall Cracking Pattern

4 PREDICTION AND ANALYSIS METHODS

4.1 Introduction

The prediction methods used to analyze the masonry walls are described in this chapter. The methods include the MSJC shear equation (2013), interaction diagram, equivalent truss model, and strut-and-tie model. The predicted strength from these methods is compared to the measured average lateral strength of the six wall specimens.

4.2 Partially-Grouted Analysis using the MSJC Code

The MSJC (2013) code details two approaches for predicting the strength of masonry shear walls: a set of equations or an axial-flexure interaction diagram. Both methods are investigated.

4.2.1 MSJC Shear Equation

The strength design procedure for shear walls is contained in section 9.3.4.1.2 of the MSJC (2013) code and is reproduced herein as Equations 4-1 to 4-3. The shear equation (Equation 4-1) combines the effects of both masonry (Equation 4-2) and reinforcing steel (Equation 4-3) as to prevent a brittle failure. The equations are based on tests conducted on fully-grouted specimens. The commentary of the code states that the grouted shear wall factor, γ_g, is used to compensate for the observed reduced strength until methods can be developed to more accurately predict the performance of partially-grouted walls. Thus, the code penalizes the shear strength of masonry walls by 25% when walls are partially-grouted. The use of a reduction factor is intended to be a

29

conservative adjustment to the masonry shear equation until further research could confirm the value of the factor or develop a new method.

$$V_n = (V_{nm} + V_{ns})\gamma_g \tag{4-1}$$

$$V_{nm} = \left[4.0 - 1.75\left(\frac{M_u}{V_u d_v}\right)\right] A_{nv}\sqrt{f'_m} + 0.25P_u \tag{4-2}$$

$$V_{ns} = 0.5\left(\frac{A_v}{s}\right)f_y d_v \tag{4-3}$$

where:

V_n = nominal shear strength

V_{nm} = nominal shear strength provided by masonry

V_{ns} = nominal shear strength provided by shear reinforcement

γ_g = grouted shear wall factor

M_u = factored moment

V_u = factored shear force

d_v = actual depth of member in direction of shear considered

A_{nv} = net shear area

f'_m = specified compressive strength of concrete masonry

P_u = factored axial load

A_v = cross-sectional area of shear reinforcement

s = spacing of reinforcement

f_y = specified yield strength of steel for reinforcement

For a cantilever wall with an applied lateral concentrate load at the top of the wall, the bending moment is simply the load multiplied by the height of the wall. For ease of calculation, Nolph (2010) made the substitutions presented in Equations 4-4 and 4-5:

$$\frac{M_u}{V_u d_v} = \frac{V_u h_w}{V_u d_v} = \frac{h_w}{d_v} \rightarrow V_{nm} = \left[4.0 - 1.75\left(\frac{h_w}{d_v}\right)\right] A_{nv}\sqrt{f'_m} + 0.25P_u \qquad (4\text{-}4)$$

$$\rho_h = \frac{A_v}{st} \rightarrow \frac{A_v}{s} = \rho_h t \rightarrow V_{ns} = 0.5(\rho_h t)f_y d_v \qquad (4\text{-}5)$$

where:

h_w = height of wall

ρ_h = ratio of reinforcement orientated horizontally

t = nominal thickness of CMU

The substitution in Equation 4-4 allows for easier calculations because only the dimensions of the wall are needed; i.e., the shear strength of the element is a function of the geometric properties of the element and not a function of the applied loads. The substitution in Equation 4-5 is useful when horizontal (or shear) reinforcement has irregular spacing, which is the case in the present study. For the analysis of the wall in this study, only the horizontal reinforcement in the masonry will be counted as stirrups. This excludes the reinforcement in the floor slabs.

The MSJC code does not directly address the shear strength prediction of walls with openings. If the openings were neglected, as shown in Method 1 of Figure 4-1, the predicted strength is 91 kips (405 kN), which is abundantly unconservative. The code, however, limits the shear strength of an element based on the ratio between the ultimate moment and the product of the ultimate shear force and depth of the wall. For the walls here considered, the maximum predicted shear, based on the imposed limit, is 18.6 kips (82.6 kN), which is 78% of average

measured strength. Although the predicted strength is reasonable, Method 1 does not account for openings in walls.

One approach to account for openings is to assume that each side of the opening act as two separate walls that are connected by the beams. The individual capacity of each separate wall could be computed and added together to calculated the predicted capacity of the entire wall, as shown in Method 2 of Figure 4-1. This method is somewhat justifiable because it was observed during testing that the panels were weaker than the beams since limited cracking occurred in the beams and substantial cracking occurred in the panel. Using this approach, the predicted shear capacity of one panel is 38.5 kips (171 kN) and the combined capacity is 77.0 kips (343 kN). This prediction is 324% of the measured average and very unconservative. The upper limit of one panel according to the ratio between the ultimate moment and the product of the ultimate shear load and depth of the wall is 7.8 kips (35 kN), which would result in a predicted shear capacity of 15.6 kips (70 kN)—66% of the measured average strength—which is an overly conservative estimate.

It is important to note that the strength reduction factors, ϕ, used within this analysis was the prescribed value of 0.8, and even with their inclusion, these original results are unconservative. The calculations for the MSJC equation are shown in Appendix C.

4.2.2 Interaction Diagram

The walls can also be modeled as cantilever beams applied with both axial and flexural loads, i.e., a beam-column. For beam-column cases, the code indicates that an interaction diagram should be developed, which, however, does not account for the openings in the walls. If the openings were replaced by ungrouted portions, the interaction diagram shown in Figure 4-2

32
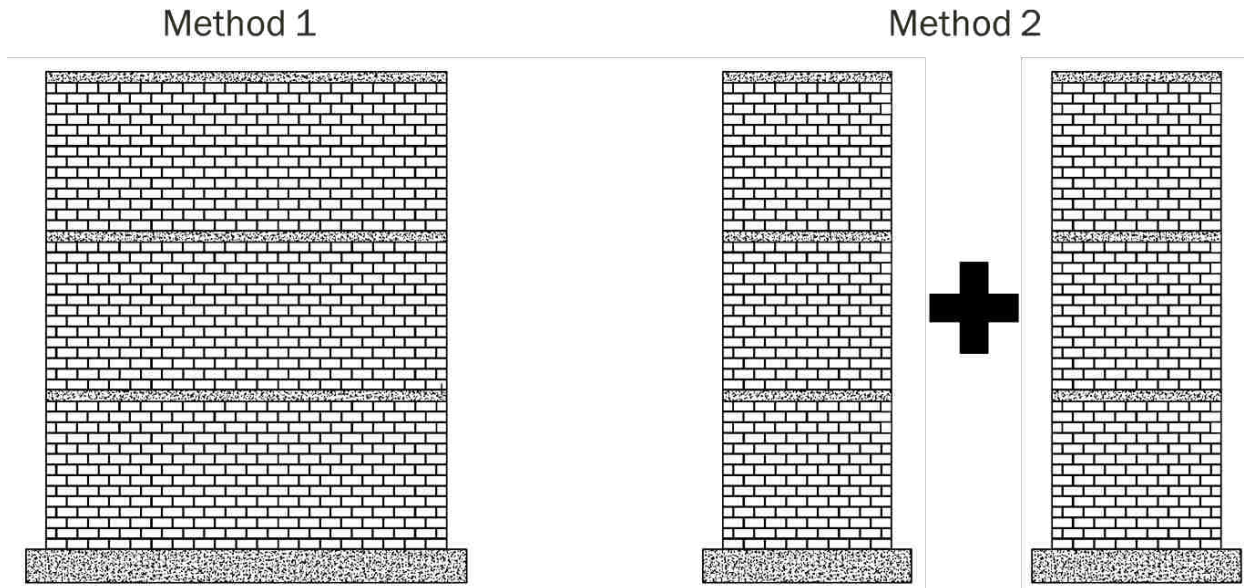
Figure 4-1: MSJC Shear Equation Modeling Methods

is obtained. Typically, an interaction diagram displays a smooth curve because the element being considered is fully-grouted. Because the walls investigated were partially-grouted, an equivalent area was determined based on the areas of the grout and CMUs. In the grouted portions, the width was the thickness of the block while in the ungrouted portions, the width was the thickness of the face shells only. The process used is similar to calculate the area of the stress block in T-beams when the depth of the stress block falls below the flange.

In an interaction diagram, the intersection between the obtained curve and the applied axial load gives the moment capacity of the element. The axial load applied on a wall was the sum of the concrete beam on top of the wall and the steel shapes used as dead weight placed on top of the wall. The concrete beam was 13 in. x 13 in. x 141.7 in. and assumed to weigh 145 lb/ft^3. The calculated axial load was 13.4 kips (59.6 kN). The intersection of this axial load and the obtained curve resulted in a moment of 427 kip-ft (579 kN-m), which corresponds to a lateral force of 31.1 kips (138 kN) applied at the top of the wall. This is 131% of the measured average wall
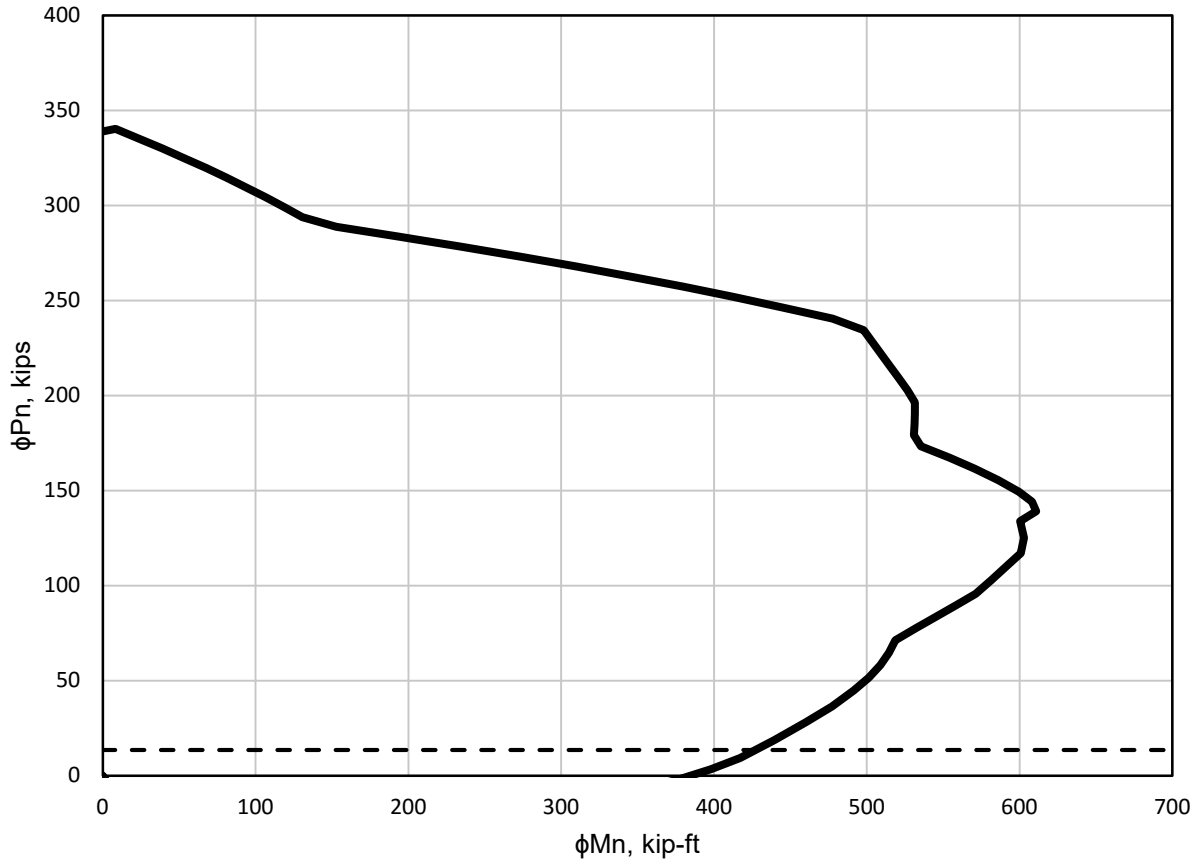
Figure 4-2: Interaction Diagram

capacity—a slightly unconservative result. If openings could be accounted for within this method, there is a possibility that the method could produce a more reasonable result.

4.3   Equivalent Truss Model

The three story walls can also be modeled as a three-bay frame (or truss) with diagonal braces in the bays representing a compressive element (strut) within the wall panels, as shown in Figure 4-3. The three-cell grouted areas on the edges of the wall and on each side of the door or window openings are modeled as columns in the frame. The beams of the model frame were the concrete slab or beam and the grouted bond beam, i.e., the T-beam shown in Figure 3-1. The webs of the T-beams over the door and window openings were deeper than the webs of the T-

34

beams on the top of the walls—they had three grouted courses compared to one grouted course. The T-beam on top of the wall, however, had thicker flange since the concrete beam was 13 in. deep and the concrete slab was only 4 in. deep. The forces applied to the column and to the beam were assumed to act through the center of mass of the reinforcing steel.

The location of the nodes was based on geometry, i.e., intersection of columns and beams. When analyzing an existing structure or tested specimen, cracking patterns may be used to determine the location of nodes and struts because those patterns indicate the flow of force (Nolph, 2010; Elmapruk, 2010). In this study, each tested wall experienced a similar pattern of diagonal cracking occurring in each "panel" from the top corner to the opposite toe. For this reason, struts were assumed to be diagonal bracing from nodal points that connected beams and columns.
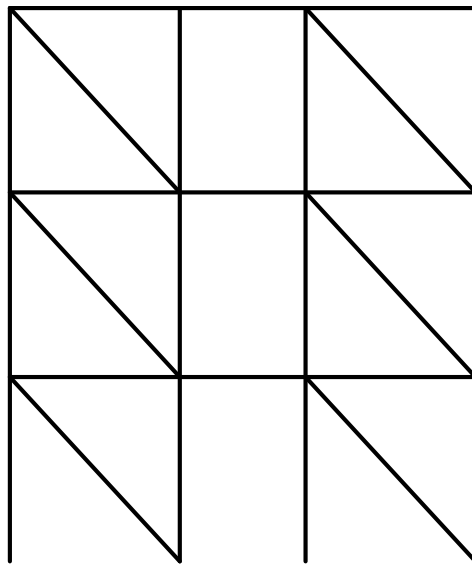
Figure 4-3: Equivalent Frame Model

The model frame described was used to conduct a pushover analysis to predict the lateral strength of the partially-grouted walls. Elmapruk (2010) and Nolph (2010) used this approach to predict the strength of their specimens. However, the authors performed several iterations whereby nodal locations were changed based on engineering judgement or to account for observations made during their testing program. In those studies, the authors postulated that the size of the brace or "strut" was dependent on the depth of the bond beam and the width of the grouted column, as depicted in Figure 4-4. The width and area of the strut were determined from Equations 4-6 and 4-7, respectively. The compressive strength and force were then calculated using Equations 4-8 and 4-9, respectively.
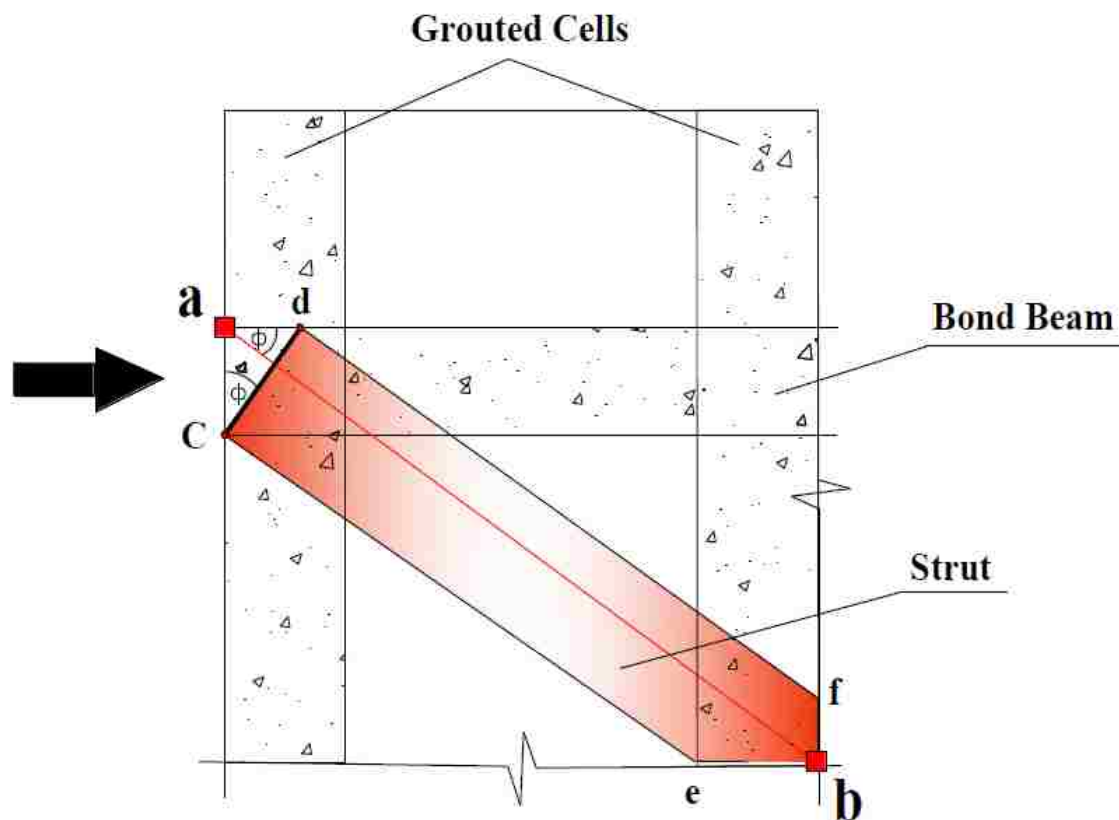
Figure 4-4: Wall Strut Calculation for Partially-Grouted Shear Walls (Elmapruk 2010)

$$w_s = cd = ca/\cos\varphi \qquad (4\text{-}6)$$

$$A_{cs} = w_s t_{sh} \tag{4-7}$$

$$f_{ce} = 0.85\beta f'_m \tag{4-8}$$

$$F_{ns} = f_{ce}A_{cs} \tag{4-9}$$

where:

w_s = width of the strut

cd = the distance from c to d.

ca = the distance from c to a

φ = the strut angle

A_{cs} = area of strut

t_{sh} = face shell thickness

f_{ce} = strut compressive strength

β = nodal efficiency factor

f'_m = masonry compressive strength

F_{ns} = maximum strut compressive force

The compressive strength of the strut is reduced by the nodal efficiency factor, β, which is 1.0 for three struts intersecting at a node, 0.8 for two struts and a tie intersecting at node, and 0.6 for one strut and two ties intersecting at a node. Ties are elements that resist tension, and in reinforced masonry ties are the reinforcement in bond beam and slabs.

For this analysis, the nodal efficiency factor was assumed to be 0.6 in order to be conservative since certain struts intersected two ties. The face shell thickness, $t_{sh,}$ was 0.64 in.; the depth of the bond beam, ca, was assumed to be the depth of the concrete slab and bond beam; and the strut angle, φ, was the angle from one node to another from the horizontal.

37

The material properties for the structural elements were based on the tested samples that are summarized in Appendix B. Average compressive strengths for masonry prisms and concrete were used as well average tensile strengths of reinforcement samples. The masonry average compressive strength, f'_m, was 1.8 ksi; the concrete average compressive strength, f'_c, was 5.4 ksi; and the average yield strength of the reinforcement, f_y, was 76.6 ksi. The masonry modulus of elasticity was 2455 ksi—determined from the tested masonry prisms. The modulus for steel was 29000 ksi and Equation 4-10 was used to calculate the concrete modulus of elasticity of 4170 ksi. The gross cross sectional areas for concrete and masonry members were either rectangular or T-shape with the moment of inertia calculated based on the orientation of these shapes. For members involving reinforcing steel, the area used was the total cross-sectional area of the reinforcement and the moment of inertia of those members considered the reinforcement.

$$E = 5700\sqrt{f'_c} \tag{4-10}$$

The pushover program required the calculation of four values: the reciprocal of the weak moment of inertia (RIBUCK), the reciprocal of the yield stress multiplied by the cross-sectional area (RF), the reciprocal of the yield stress multiplied by the plastic section modulus (RM), and the reciprocal of the shear force multiplied by the shear area (RV). The value of RIBUCK was set zero for all members to prevent buckling. The value of RF was calculated by taking the inverse of the product of the cross-sectional area and the yield stress of the reinforcement (for steel members) or the maximum compressive stress (for concrete or masonry members). The value of RM was calculated by taking the inverse of the product of the section modulus and the yield stress or the maximum compressive stress. The value RV was calculated by taking the inverse of the product of two-thirds of the maximum shear force. For steel members, the maximum shear force was calculated by multiplying the cross sectional area by the yield stress.

38

For masonry members, the maximum shear force was calculated using the masonry component of the MSJC shear equation (Equation 4-2). The maximum shear force for concrete members was calculated using the sum of ACI Equation 11-3 and ACI Equation 11-15, shown herein as Equations 4-12 and 4-13, respectively (McCormac and Brown 2013).

$$\phi V_n = \phi(V_c + V_s) \tag{4-11}$$

$$V_c = 2\lambda\sqrt{f'_c}b_w d \tag{4-12}$$

$$V_s = \frac{A_v f_{yt} d}{s} \tag{4-13}$$

The connections between columns and beams were assumed as rigid while the connections for the struts were assumed as pinned. The reason was to account for the rigid-like nature of the walls. The connection of the columns to the foundation was also assumed to be rigid.

The frame model shown in Figure 4-3 was analyzed using a nonlinear pushover program (Balling 2012). The inputs are summarized in Appendix D. A load was applied to the top left node of the frame and the load was steadily increased. When an element reached its capacity, that element was replaced, within the program, by an equivalent force. The procedure was repeated until the structure was unstable. The results are shown in Figure 4-5. Two analyses are shown: one that included and one that excluded the concrete floor slab into the calculations for the width of the strut.

In the linear regime, the pushover curves have a similar slope as that of the loading envelope of the walls. However, as the responses become nonlinear, the calculated results levels out while the actual wall continues to resist additional load. The increasing resistance may be due to the strain hardening in the reinforcement, which was not considered in the model frame. The
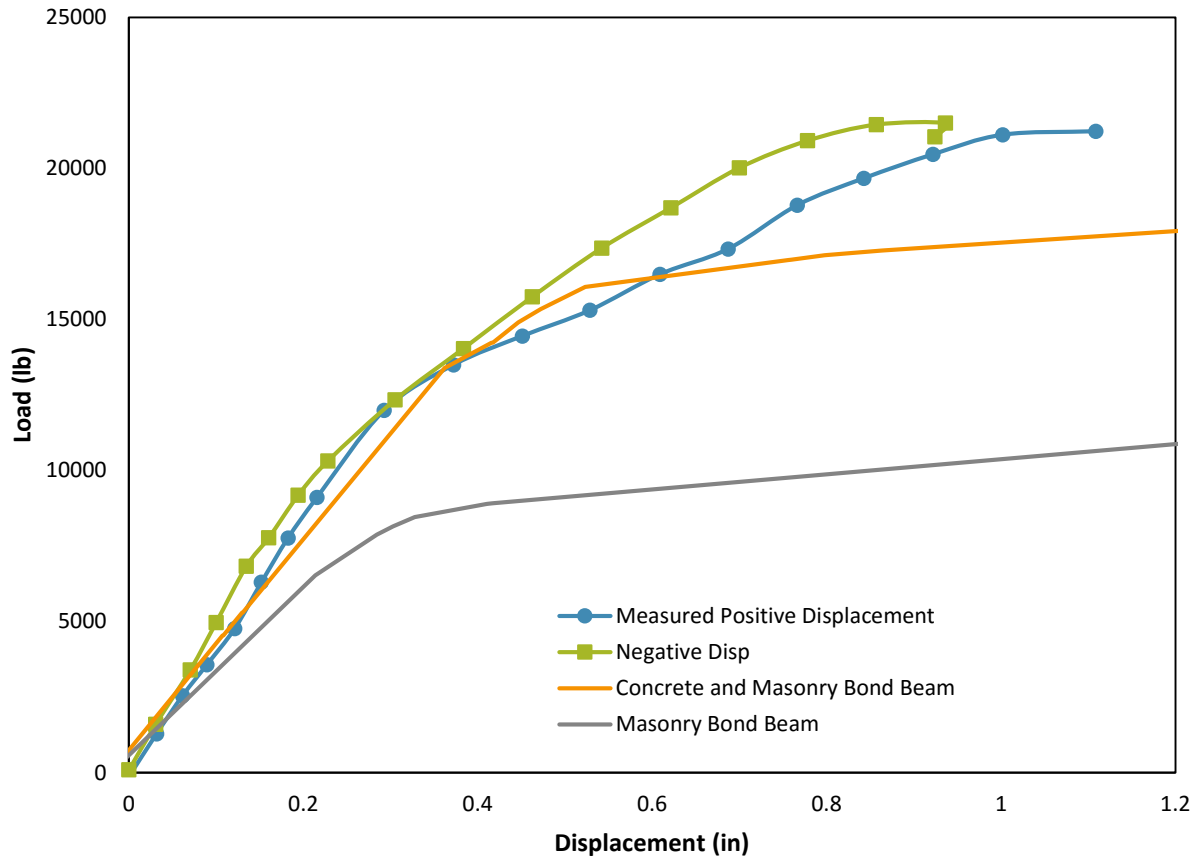
Figure 4-5: Wall 5 and Equivalent Frame Pushover Curves (1)

response of the model that incorporated the concrete floor slab and the masonry bond beam into the calculations for the width of the strut is very reasonable.

Even though the responses of the models are similar in the linear regime and the early parts of the nonlinear regime to that of the measured response, the model continues to resist load well beyond the maximum measured displacement, as shown in Figure 4-6. While the lateral displacement of 1 inch is reasonable for the experiments, the model predicts a maximum lateral displacement of approximately 18 inches, which is unreasonable for masonry walls. Additionally, the model continues to experience an increase in load even after the specimen had failed. The wall, whose response is shown in Figure 4-6, had a measured strength of 21.9 kips

(97 kN) while the model predicts a capacity of 23.5 kips (105 kN). While the predicted value is close to the average of the six walls, it does not reach that value until it had displaced an unreasonable amount.
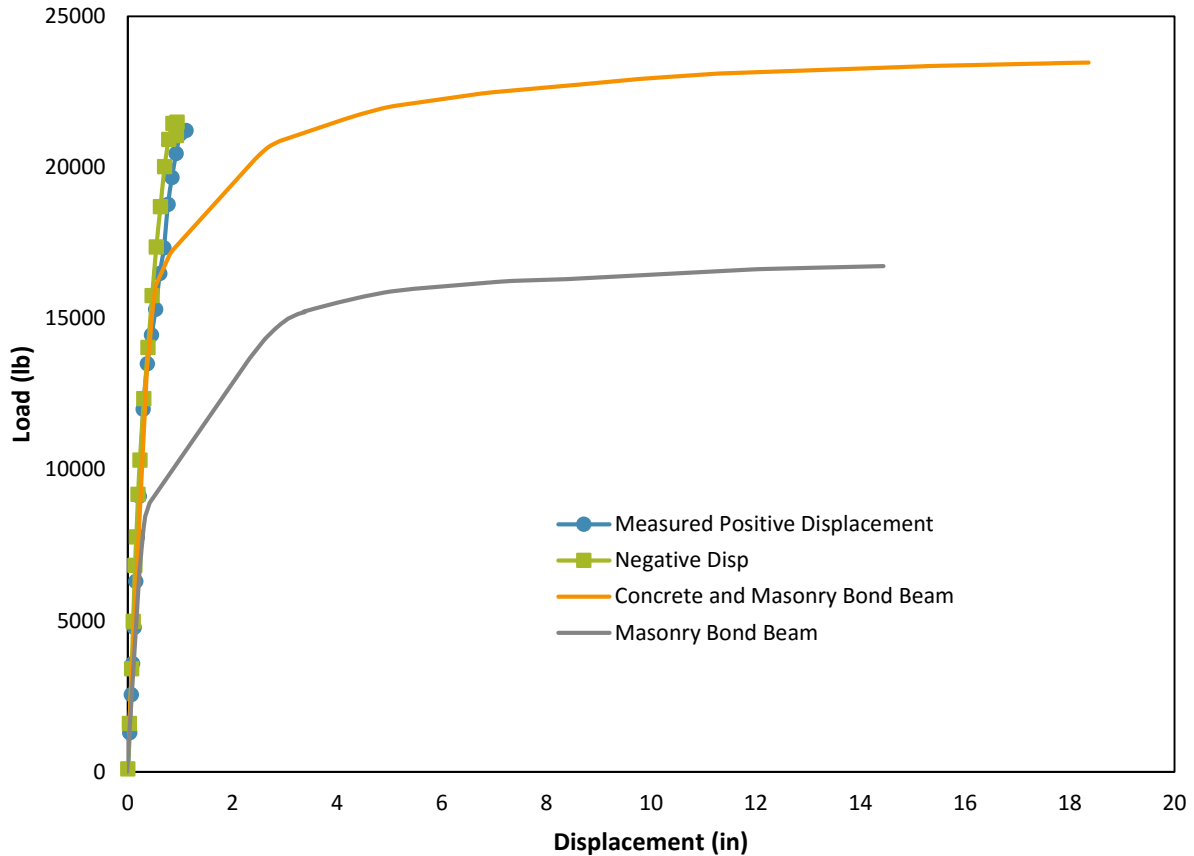
Figure 4-6: Wall 5 and Equivalent Frame Pushover Curves (2)

A summary of the pushover analysis results is presented in Table 4-1. The first strut reached its compressive strength at 11.9 kips and the compressive strength of the last strut to reached its capacity was 17.3 kips. Nolph (2010) stated that a model failed under the applied loading when the force in any strut was approximately the strength of the compression strut. The author also stated that if a tie yielded prior to the failure of a strut, the tie should be replaced by a force equal to the yield strength of the tie. The analysis would continue until a strut failed.

Table 4-1: Pushover Analysis Output

Load (kip)	Load (kN)	Member	Member Type	Failure
11.87	52.8	9	Strut	compression yield
14.93	66.4	18	Strut	compression yield
15.29	68.0	27	Strut	compression yield
16.07	71.5	4	Strut	compression yield
17.14	76.2	13	Strut	compression yield
17.29	76.9	22	Strut	compression yield
20.26	90.1	5	Beam (tie)	negative hinge
20.43	90.9	7	Beam (tie)	negative hinge
20.61	91.7	5	Beam (tie)	negative hinge
20.66	91.9	2	Beam (tie)	negative hinge
20.73	92.2	2	Beam (tie)	negative hinge
20.88	92.9	7	Beam (tie)	negative hinge
21.59	96.0	14	Beam (tie)	negative hinge
21.74	96.7	16	Beam (tie)	negative hinge
21.76	96.8	14	Beam (tie)	negative hinge
21.94	97.6	16	Beam (tie)	negative hinge
21.99	97.8	11	Beam (tie)	negative hinge
22.04	98.0	11	Beam (tie)	negative hinge
22.45	99.9	12	Column	positive hinge
22.49	100.0	21	Column	positive hinge
22.76	101.2	1	Column (tie)	positive hinge
22.93	102.0	26	Column	positive hinge
23	102.3	3	Column	positive hinge
23.11	102.8	8	Column	positive hinge
23.12	102.8	17	Column	positive hinge
23.37	104.0	24	Column (tie)	positive hinge

The main issue with replacing tension ties that have yielded with an equivalent force is that nonlinear behavior of the wall is not captured. The omission of nonlinear behavior, although conservative for design, neglects important information regarding the response of the wall to lateral loading. Moreover, the pushover analysis used is applicable to steel structures because its stress-strain curve can be represented by a linear regime and a constant nonlinear regime as

42

shown in the schematic in Figure 4-7. The stress-strain relationship for cementitious materials is more rounded because of cracking. In order to better predict the strength of masonry shear walls using a pushover analysis, the stress-strain relationship of the masonry must be considered.
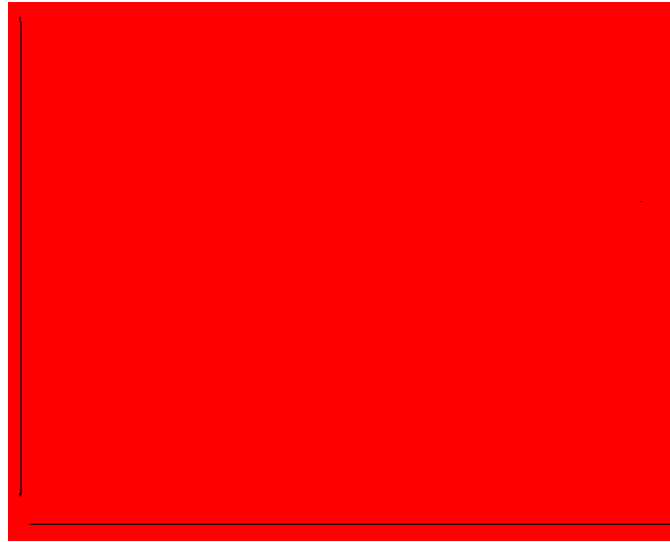
Figure 4-7: Steel and Concrete Stress Vs Strain Curves

4.4 Strut-and-Tie Model

4.4.1 Equivalent Truss Model vs. Strut-and-Tie Model

While there have been modifications of the strut-and-tie procedure that was first introduced by Schlaich et al. (1987), many of these should be classified as equivalent truss designs. One of the reasons is that these modifications do not sufficiently accommodate the width of the strut. Under a lateral load, struts terminate in the toe of the wall along the line of action. In the strut-and-tie methodology, the struts must be aligned such that they do not cross each other and that their individual widths are accommodated. Such a requirement differs from that of an equivalent truss designs in that all struts end at the same node, which is the traditional structural analysis methodology. This difference in modeling procedures is depicted in Figure 4-8.

43
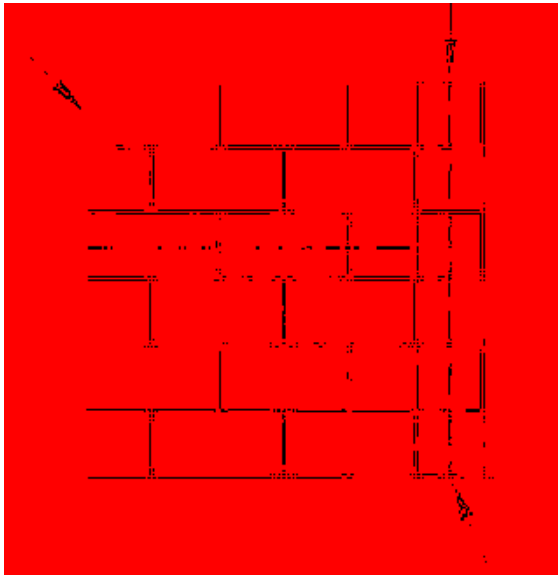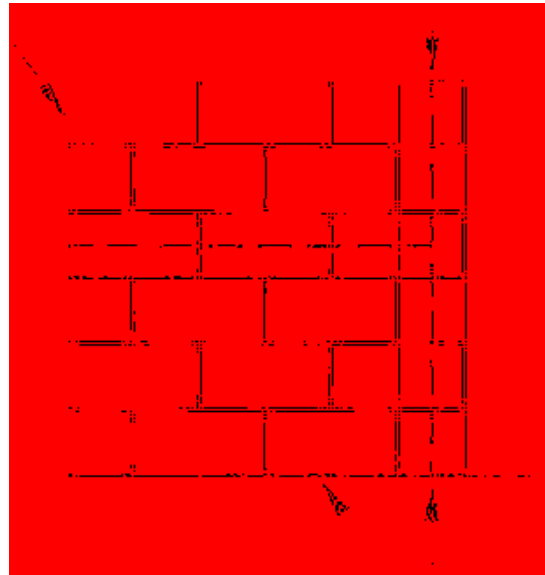
(a) Equivalent Truss   (b)Strut-and-Tie

Figure 4-8: Modeling Procedures

The methodology of Elmapruk (2010) and Nolph (2010) for determining the width of the strut was unconventional compared to other strut-and-tie procedures because the width of every strut was based on the depth of the bond beam. That approach neglected the nodal zone procedures, which considers the strength of intersecting struts and ties—an important and necessary condition of the strut-and-tie procedure in order to maintain equilibrium. In addition, the depth of the bond beam may not be well defined. The walls tested and analyzed by Elmapruk (2010) and Nolph (2010) were one story high and were not topped with a floor or roof slab. In the study presented herein, calculations were performed considering the depth of the bond beam and floor slab and the depth of the bond beam only—the former producing the more accurate results.

Elmapruk (2010) and Nolph (2010) were also unique in that their analysis was performed using pushover analysis software. Because of the simplified strut width assumption, the analysis

www.manaraa.com

was streamlined. That methodology could be used to show the degradation of the elements of the frame model and may even correlate to measured results. In most cases, the analysis conducted by Elmapruk (2010) and Nolph (2010) ended when the strut in the bottom corner opposite to that where the load was applied reached its strength—a failure characteristic of a pushover analysis of a frame where a large portion of the lateral load is transferred to that member. The pushover analysis presented in this study also ended due to the aforementioned failure.

4.4.2 Strut-and-Tie Model Properties

The underlying principle of the strut-and-tie methodology is to simplify the analysis of a complex structure by dividing the structure into compression and tension elements that intersect at nodes. The strut-and-tie modeling procedure is an iterative process that does not involve a pushover analysis but involves changing the location of nodes and the distribution of forces until equilibrium is obtained. In shear walls, the predicted strength of the wall is determined by calculating the lateral load capacity of the struts. The strength of these struts is based on the strength of the masonry, the inclination of the struts, and the strength of the ties. A typical strut is shown in Figure 4-9 and its strength is calculated using Equations 4-14 through 4-21.

The location of nodes and struts is based on engineering judgement and the best design is usually the simplest due to the principle of minimum strain energy. Once the nodal zones and struts have been laid out, the vertical load is applied to the top of the struts. If the node includes vertical reinforcing steel, the vertical force, F_y, is the sum of the applied vertical load and the tension force in the reinforcing steel.

45
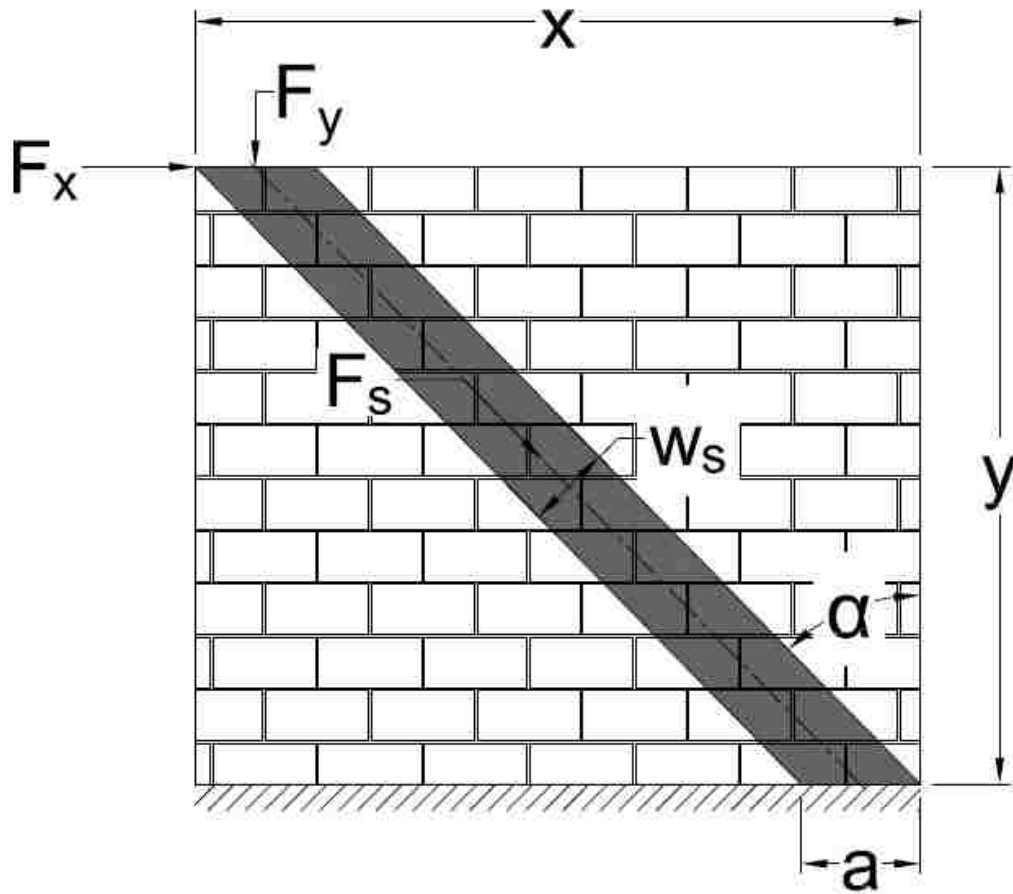
Figure 4-9: Strut-and-Tie Illustration

$$w_s = \frac{F_s}{0.8 t_s f_{ce}} \tag{4-14}$$

$$F_s = \sqrt{F_x^2 + F_y^2} \tag{4-15}$$

$$F_x = F_y \tan\alpha \tag{4-16}$$

$$\alpha = \tan^{-1}\frac{x-a}{y} \tag{4-17}$$

$$f_{ce} = min \begin{Bmatrix} 0.8\beta_n f'_m \\ 0.8\beta_s\beta_\alpha f'_m \end{Bmatrix} \tag{4-18}$$

$$\beta_n = \begin{Bmatrix} 1.0 \; for \; C-C-C \\ 0.8 \; for \; C-C-T \\ 0.6 \; for \; C-T-T \end{Bmatrix} \tag{4-19}$$

46

$$\beta_s = \left\{ \begin{array}{c} 1.0 \; for \; prismatic \\ 0.8 \; for \; struts \; that \; cross \; 1 \; stirrup \\ 0.6 \; for \; struts \; that \; cross \; no \; stirrups \end{array} \right\} \qquad (4\text{-}20)$$

$$\beta_\alpha = \left\{ \begin{array}{c} 1.0 \; for \; \alpha = 0 \\ \frac{2}{3} \; for \; \alpha \geq 35 \end{array} \right\} \; linearly \; interpolated \; in \; between \qquad (4\text{-}21)$$

The process for determining the width of the strut begins by making an assumption for the horizontal component, a, of the strut width. The angle, α, is calculated using Equation 4-17 along with the horizontal component of force, F_x, which is calculated using Equation 4-16. The force in the strut, F_s, is then calculated using Equation 4-15 and finally the strut width, w_s, is determined using Equation 4-14. A new horizontal component of the strut width, a, is then calculated based on the strut width just determined and the strut angle. The process is iterated until convergence is reached. The strength of the strut is the minimum of either the maximum strut strength or the maximum nodal strength, both of which involve the adjustment factors given in Equation 4-18. These factors are the nodal efficiency factor, β_n, the strut efficiency factor, β_s, and the strut inclination factor, β_α; which are calculated using Equations 4-19, 4-20, and 4-21, respectively.

There are additional rules that govern the layout of struts and ties. Struts may cross ties, but cannot cross each other. In some instances, it is advantageous for a strut to cross a tie rather than have a tie contribute to the strength of the system in order for the strut efficiency factor to be increased from 0.6 to 0.75. Also, the ties cannot contribute more than they have strength. A tie can contribute until it yields, meaning $0 \leq F_s \leq F_y$, where F_y is the yield strength of the tie, i.e., the reinforcement. Groups of ties in adjacent cells can be assumed to act as one tie in order to simplify the analysis. Such an approach was especially helpful within this study because of the group of three reinforcing bars placed on the edges of the wall and next to the openings. There

47

are no limits on the width of a strut except for the size of the wall. Typically, that limit does not govern because the strength of the tie is the limiting factor.

Dillon (2015) observed another phenomenon exclusive to partially grouted walls, which he termed *toe extension*. Dillon (2015) explains, "It was hypothesized that since the end cells of the wall were always grouted and the effective thickness of the wall for the final half-block length was much greater than that of the ungrouted wall panels, it was possible that the stress fields in the grouted jamb were able to take a steeper descent to the wall toe. This would have the same effect as that of lengthening the wall, which would essentially increase the strut angle for any struts constrained by the wall edge, increase the struts' lateral force components, and thus, increase the overall strength capacity of the model." This phenomenon is depicted in Figure 4-10 and closely matches the cracking inclination observed in the walls specimens, as shown in Figure 4-11. The effective toe of a partially grouted wall can be calculated using Equation 4-22. In the model presented herein, the distance between the centroid of the flexural reinforcement and the nearest wall edge, d', was assumed to be the distance from the edge of the wall to the center of the grouted section because the last three cells were grouted unlike other studies where only the last cell is grouted.

Wall openings complicate the analysis of masonry walls using traditional methods, but can be simplified using the strut-and-tie procedure. Struts cannot pass through openings (because there is no masonry in the opening to resist the compressive force) and must, therefore, go around the opening. Walls with openings can be modeled as two walls panels connected by a beam or lintel, which perspective is similar to that of the equivalent frame design except that in a strut-and-tie model, the width of the struts must be considered in the layout of struts and ties especially at the leading toe of the wall.

48
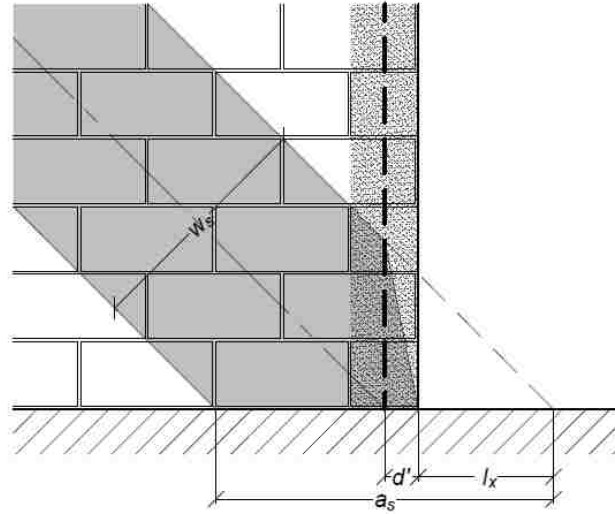
Figure 4-10: Toe Extension in Partially-Grouted Walls (Dillon 2015)

$$l_x = \frac{l_b}{4}\frac{t-t_{sh}}{t_{sh}} \equiv d'\frac{t-t_{sh}}{t_{sh}} \qquad\qquad (4\text{-}22)$$

where:

l_b = length of the whole masonry block

t = outside thickness of the wall

t_{sh} = total (face) shell thickness of the wall

d' = distance between the centroid of the flexural reinforcement and the nearest wall edge

Table 4-2 summarizes the material properties and parameters used for the strut-and-tie model presented herein. The average yield strength of the reinforcing steel was 76.6 ksi and the masonry strength used was the average ungrouted masonry prism strength from Wall 4. Only samples tested in conjunction with this wall were used because the tests more closely aligned

with the requirements of the ASTM standards. The results of the samples corresponding to the

other walls were compromised by improper testing techniques.
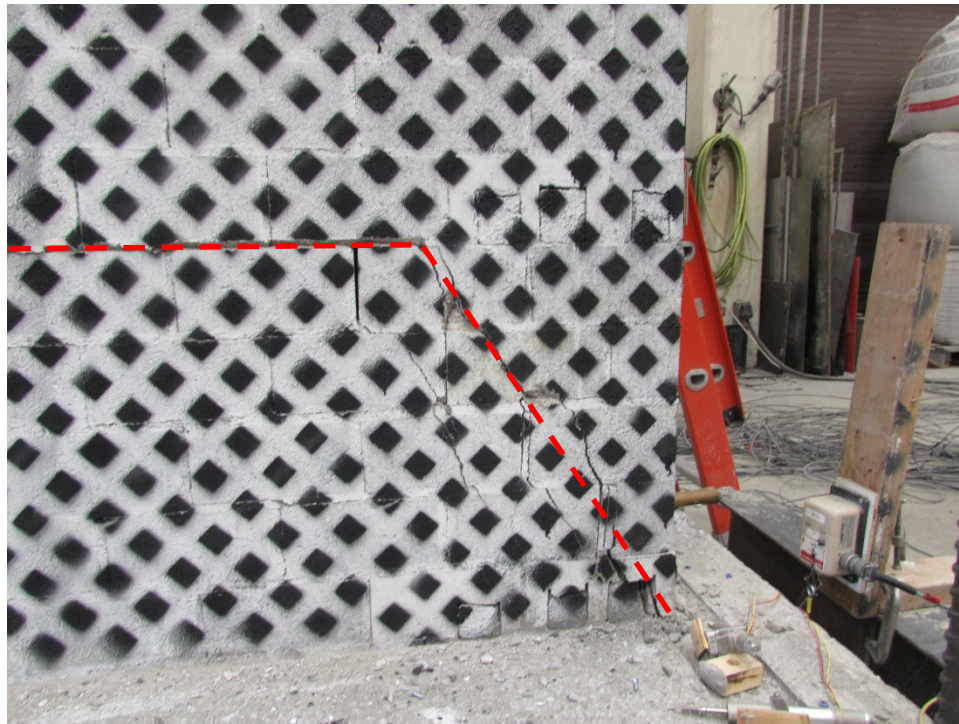
Figure 4-11: Cracking Pattern at the Toe of the Wall

Table 4-2: Strut-and-Tie Parameters

Parameter	Value	
F_y	76.6	ksi
$A_s F_y$	25.3	kip
f'_m	1803	psi
t_{sh}	1.29	in
t	3.54	in
l_x	9.64	in
P_{total}	13.4	kip
β_s	0.75	
β_n	0.8	
	0.6	

50

4.4.3 Development of Strut-and-Tie Model

An effective strut-and-tie model is usually the simplest in order to satisfy the principle of minimum strain energy. Dillon (2015) observed that this equates to utilizing as few ties as possible. The author detailed seven guiding principles when laying out the strut-and-tie model for masonry shear walls.

1. Resolve the distributed axial load into point loads and place them at discrete locations along the top of the wall. These locations are most often at the centerline of the vertical reinforcing bars, but can be any location according to engineering judgement. Typically, the magnitude of the point load is determined based on tributary length.

2. Calculate the anchorage lengths for the horizontal reinforcing steel. Reinforcing bars must have sufficient anchorage such that the tensile force does not cause the reinforcing steel to pull out. This is of concern at leading edges of shear walls where the horizontal component of the strut width must be equal to or greater than the reinforcing steel development length.

3. Layout struts from the predetermined nodes and the toe of the wall such that each strut will enter the toe sequentially without overlapping. The thickness of the leading strut, i.e., the far left or right strut terminating closest to the toe, is calculated first and then the width of the others in order from which they enter the toe. If an adjustment is made to the widths of any strut during the process, the struts behind it are moved in order to prevent struts from overlapping each other.

4. In the case of partially-grouted walls, struts originating and terminating within the grouted portion of the wall (typically along the leading edge), are calculated using the grouted thickness i.e., the thickness of the wall. The width of all other struts are calculated using the shear thickness, t_{sh}, which is the thickness of the face shell. The length of struts that cross from the ungrouted portion of the wall into the leading grouted portion will be modified by the toe extension factor, but the extension begins at the trailing edge of the strut(s) in front of it.

5. Once the model is in equilibrium from the applied axial force, the contribution from the vertical reinforcement is added. This begins at the trailing most vertical bar whereby a tensile load is induced into the reinforcement, which in turn increases the vertical component in the strut. This in turn increases the force within the strut and increases the shear force it carries. The process continues with the other vertical bars until an optimum model is achieved. Typically, in a solid wall, i.e. walls without openings, with multiple vertical reinforcing bars, the tensile load in the trailing bar is increased until the bar yields. Subsequent reinforcement may or may not be induced to yielding. This is because as vertical load applied to leading struts increases, the widths of the struts must increase and as a result, trailing struts are "pushed back." Consequently, trailing struts have a lower horizontal force component and, the model is not as optimum. This is analogous to reinforced masonry beam design principles wherein the reinforcing steel furthest away from the neutral axis yields first followed by the next furthest reinforcing bar from the neutral axis.

6. When the trailing end of a horizontal reinforcing bar is anchored to a vertical bar, the vertical component of the descending strut must be subtracted from the peak contribution of the bar at its top. This means that the two struts "share" a tie. Therefore, a tie yields once the sum of the vertical component in each of the struts equals the tensile strength of the tie.

7. The model is complete when the forces are in equilibrium, the strength of all materials are greater than their internal forces, the anchorage requirements are met, no two struts cross or overlap, and the model strength is maximum. Other variations of the model may be investigated (e.g., by changing the amount and placement of vertical and/or horizontal reinforcement) to determine the optimal model for the design scenario.

The strut-and-tie model developed for the walls in this study followed these guiding principles with some minor exceptions as explained below. Because of the openings in the walls, the general layout of the struts, ties, and nodal zones consisted of placing the nodal zones at the intersection of vertical and horizontal reinforcement in the floor slabs as shown in Figure 4-12. Such a layout allowed the force to travel from the upper left corner of the wall, down through the panel, to the reinforcement in the 2nd floor slab. At this nodal zone, a portion of the force was carried by the horizontal tie back to the trailing edge of the wall or wall opening and the remaining force was transferred to a new strut that extended towards the next nodal zone in 1st floor slab. The same load transfer procedure continued from the 1st floor slab to the bottom story where the strut extended towards the toe of the wall without crossing or overlapping the two other struts. The struts on the left side of the wall are arranged in this pattern.

The struts on the right side of the wall follow the same pattern except for the strut in the third story. Because there is "space" above the door (or window) openings, the strut can begin above the opening which means that the vertical component of the strut only comes from the applied vertical load. In contrast, the vertical component of the upper strut of the left panel comes from the vertical load and the tension in the tie. This set up is advantageous because the angle of the upper right strut is increased, which increases the lateral strength of the model. Also, only the two bottom struts contribute to the tension in the vertical tie to the right of the opening, allowing for the struts to resist an added portion of force and increasing the lateral strength of the model.

After a strut formed into a node, the resulting strut was assumed to begin from the altered strut's centerline towards the toe of the wall. Adequate space was provided to struts traversing from upper stories such that struts from lower stories did not cross each other.

Once the struts and ties layout was constructed, the calculations were as follows:

1. The axial load was applied to the two struts in the third story based on tributary length.

2. The development length for the horizontal reinforcing bar was calculated to be 16.3 in. (413 mm) and the widths of struts terminating at the leading edge of the wall were checked against this value.

3. The length of strut 6 was calculated using Equation 4-23 such that it traversed above the opening as shown in Figure 4-13 (the length of the panel is 1515 mm and from the top of the opening to the tie is 1078 mm):

$$x = y\left(\frac{1515mm + l_x - a_0}{1078mm}\right) + a_0 \tag{4-23}$$
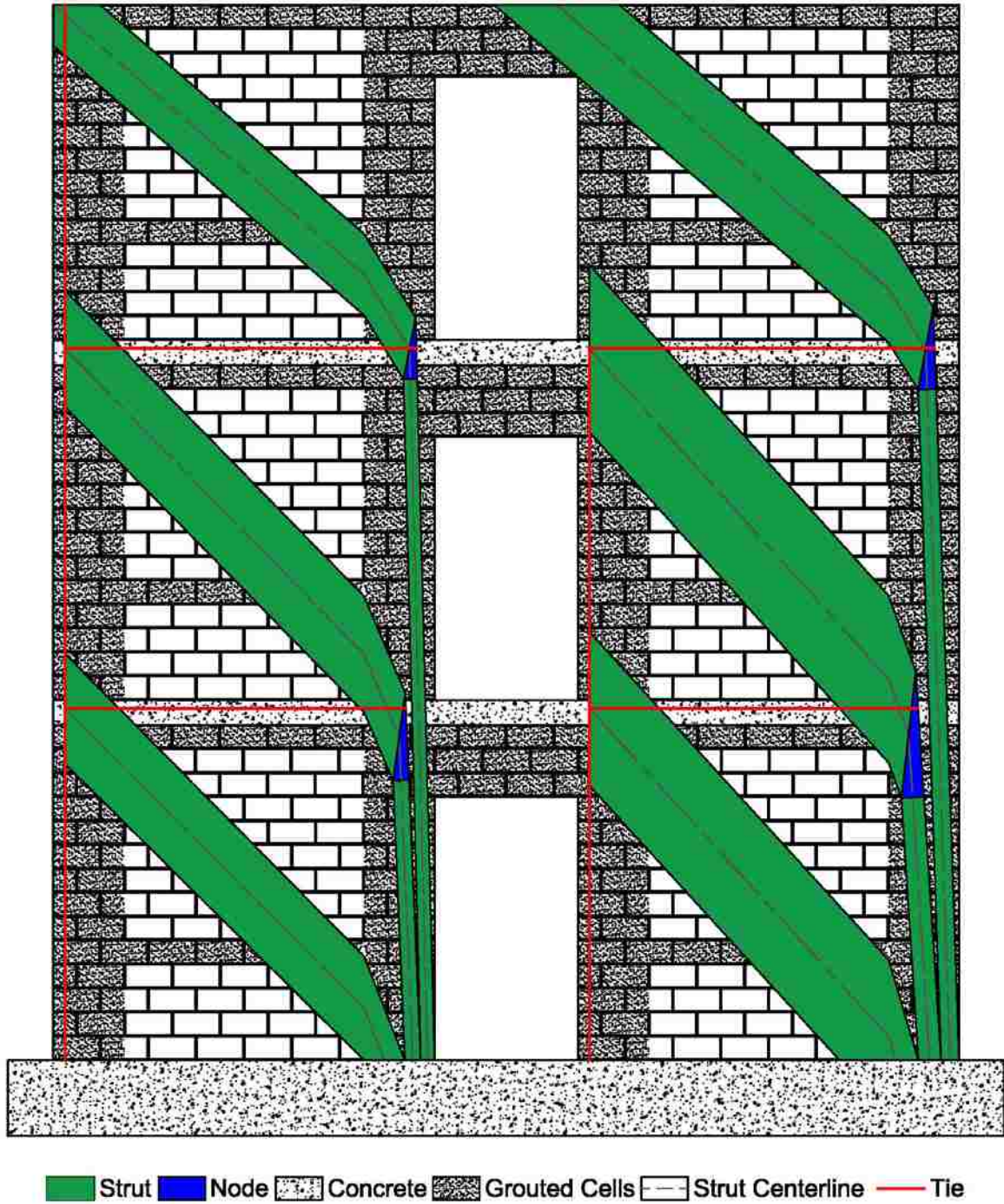
Figure 4-12: Strut-and-Tie Model

4. The horizontal length of struts 3, 5, 8, and 10 were adjusted to allow space for the struts from upper stories at the leading edge of the opening or toe of the wall. Equation 4-24 was used to calculate the length of struts 3 and 8 and Equation 4-25 was used to calculate the length of struts 5 and 10. Subscripts "i" and "j" refer to values from struts from the stories above the story being considered.

$$x = 1515mm - 45mm + l_x - x_i + y \tan \alpha_i + \frac{a_0}{2} \tag{4-24}$$

$$x = 1515mm - 45mm + l_x + \frac{a_0}{2} - a_i - a_j \tag{4-25}$$
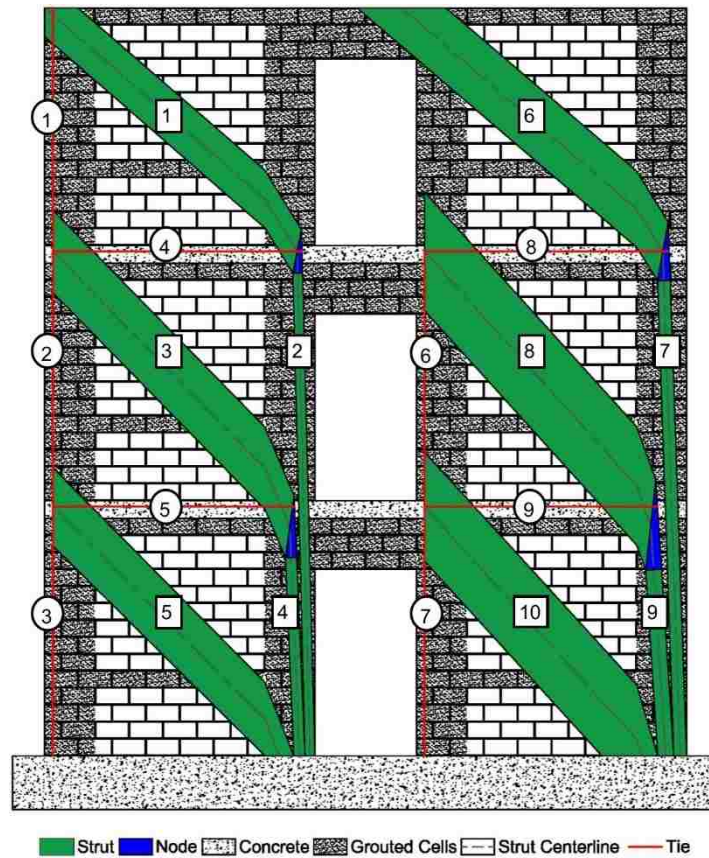
Figure 4-13: Labeled Strut-and-Tie Model

5. The horizontal lengths of the resultant struts 2, 4, 7, and 9 were determined by calculating the position of the strut centerline from the previous strut using Equations 4-26 and 4-27.

$$x = c' + \frac{a_0}{2} - a_i \tag{4-26}$$

$$c' = w_c - \left(y - \frac{x - w_c - l_x - a_0}{\tan \alpha} - \frac{w_s}{2 \sin \alpha}\right) \frac{w_c}{l_w} \tag{4-27}$$

where:

a_i = horizontal width of strut from upper stories if applicable

6. The effect of the coupling beam was accounted for by adding the strength of a stirrup in each of the lintels to the total tie strength of the vertical reinforcement to the right of the opening. This was accomplished by adding two times the stirrup strength to the total tie strength and then adding the tie strength to the vertical component of strut 6. The strength of a stirrup was calculated by multiplying the cross sectional area of the stirrup to its yield strength. The resulting value was 2.39 kips (10.65 kN).

7. Struts widths were iterated in the following order: 6, 7, 8, 9, 10, 1, 2, 3, 4, and 5. The reason the struts in the right side of the wall were balanced first was that the strength of strut 6 was based only on the applied axial load. A strut is balanced when its width is sufficient to carry the applied force. Figure 4-14 shows the balanced state of the strut-and-tie model with initial conditions. The axial load was first calculated based on tributary length; however, the applied axial load to strut 6 was increased by the ratio in Equation 4-28 until the sum of the forces in ties 6 and

7 was equal to its strength, i.e., the reinforcing bar yielded or the total axial load was reached as shown in Figure 4-15.
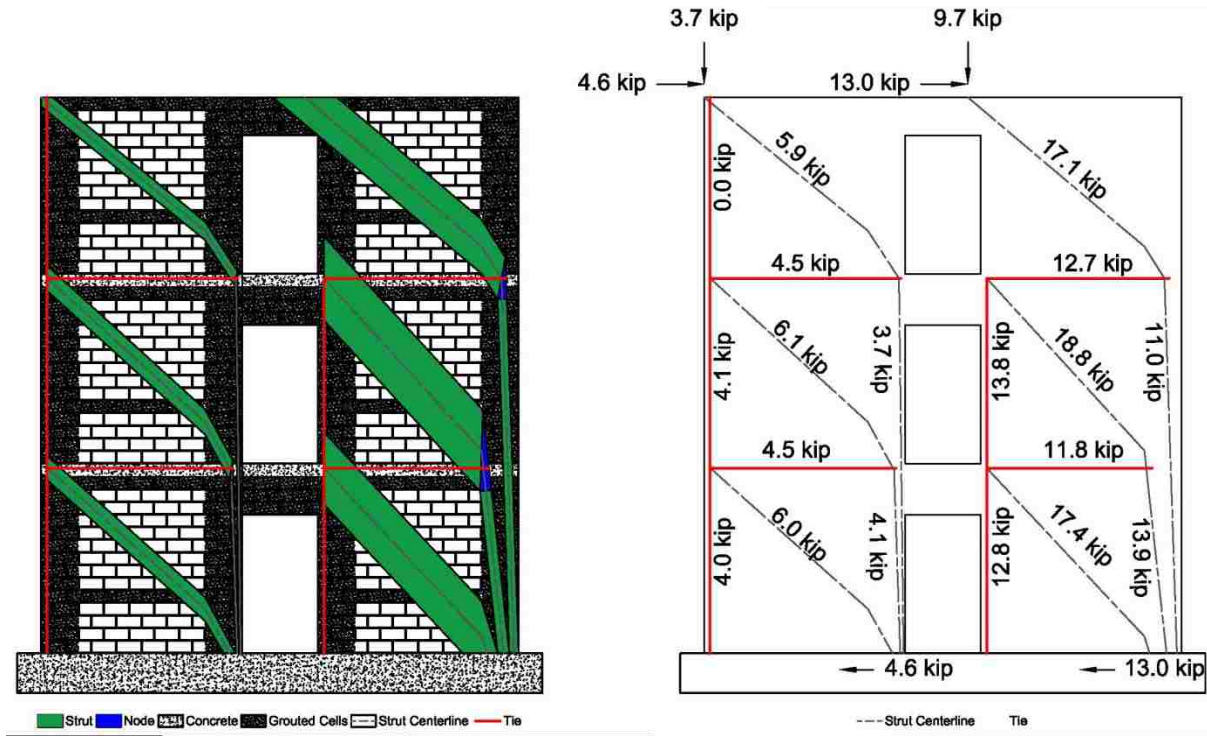
Figure 4-14: Initial Conditions of Strut-and-Tie Model

$$P_{new} = (1 + \frac{A_s F_y - A_s F_s}{A_s F_y})P_0 \qquad (4\text{-}28)$$

where:

A_s = area of steel

F_y = yield strength of steel

F_s = force in steel

P_0 = original force applied to strut

P_{new} = new force applied to strut
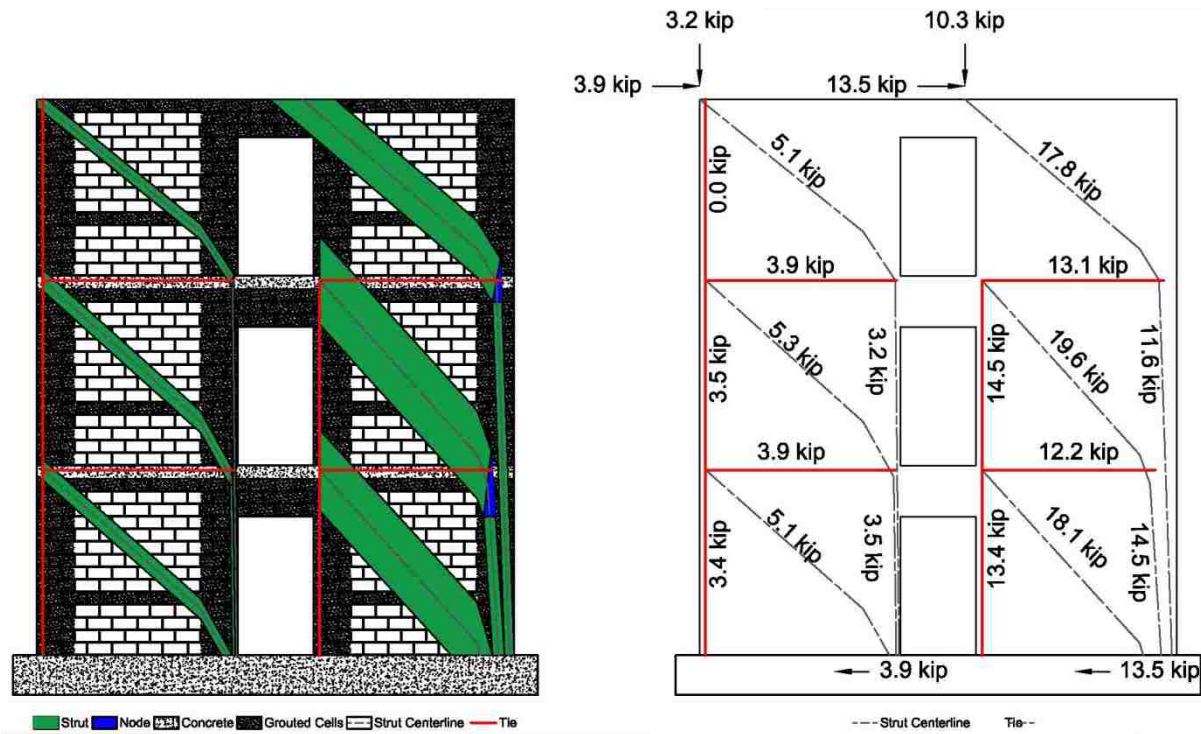
Figure 4-15: Intermediate Strut-and-Tie Model (59th Iteration)

8. The applied axial load on strut 1 was equal to the total axial load minus the axial
   load placed on strut 6. The contribution from the tie on the trailing edge was
   increased until it yielded. Once all of the forces were in equilibrium, the model was
   complete as illustrated in Figure 4-16. The calculations for several iterations of the
   strut-and-tie model are summarized in Appendix E.

4.4.4   Strut-and-Tie Model Results

   After a number of iterations of nodal locations and strut configurations, Figure 4-16 shows

one optimum design. When using the parameters from the component tests and both the strut

efficiency and nodal efficiency factors as aforementioned, the strut-and-tie analysis predicted the

lateral strength of the wall to be 23.6 kips (105 kN), which is 99.6% of the average. There is,

www.manaraa.com
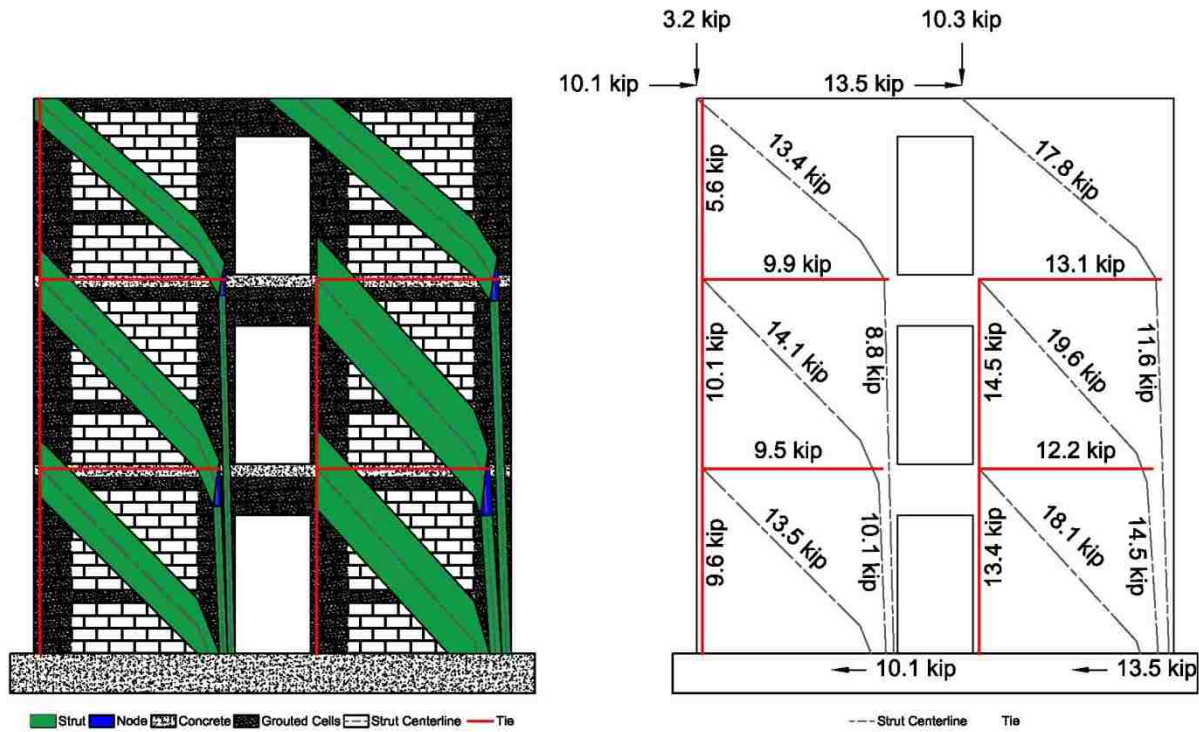
Figure 4-16: Optimized Strut-and-Tie Model

however, a possibility for other optimum designs, which is the "two-edged sword" of an analysis using strut-and-ties models.

The same model developed for walls with door openings can be used for walls with window openings because the struts collect at the toe or the opening (in the case of the door) or directly below the opening (in the case of the window) as shown in Figure 4-12 and Figure 4-17, respectively. If the wall was just one story high, the strut on the left side could travel beneath the window opening, which would result in an increase in lateral strength as compared to a door opening, where the strut will end at the opening. Voon and Ingham (2008) observed that for one story high walls, the smaller openings resulted in smaller decrease in lateral wall capacity while the larger openings resulted in larger decrease in wall strength. In the case of multistory walls, this effect is negated because struts from above stories collect at the edge of openings and

60
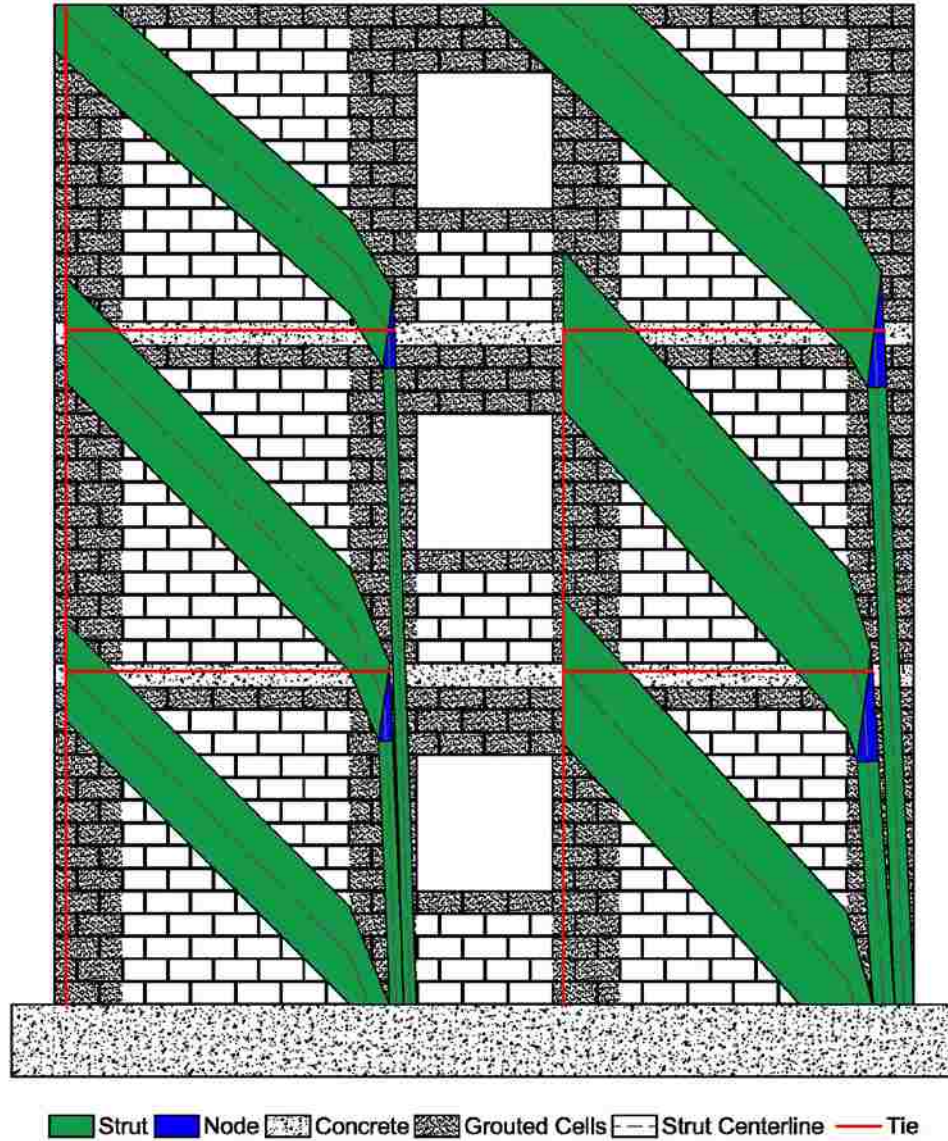
Figure 4-17: Strut-and-Tie Model for Walls 4 and 7

typically do not go under the openings. This is most likely the reason the average strength for the walls with doors and that for walls with windows was similar.

Walls 4 and 7 had reinforcement directly underneath the window that did not extend to the edges of the wall; however, the reinforcement in Wall 10 did extend to the edges of the wall. This difference may account for the average strength of Walls 4 and to be slightly less than Wall 10 (22.6 kips vs. 24.8 kips). If Wall 4 and 7 were removed from the set of walls, the average

strength would increase to 24.3 kips (108 kN) and the capacity predicted by the model would be 97.4% of the measured average strength. The decrease in strength for Walls 4 and 7 is because the compressive forces in the panels do not cross any reinforcement and allow the energy to dissipate throughout—decreasing the efficiency of the panel. In the analysis, this behavior is modeled by changing the struts from being prismatic to bottle-shaped, as illustrated in Figure 4-18, and was accounted for by decreasing the strut efficiency factor, β_s, from 0.75 to 0.6. The predicted strength for Walls 4 and 7 would decrease to 23.3 kip (102 kN) as illustrated in Figure 4-19, which is 102.7% of the average measured strength for these wall. Note that in the figure, the struts are not shown as being bottle-shaped. Although the obtained result for these walls is reasonable, more research is needed to better account for this behavior.

(a) Prismatic Strut   (a) Bottle-Shaped Strut
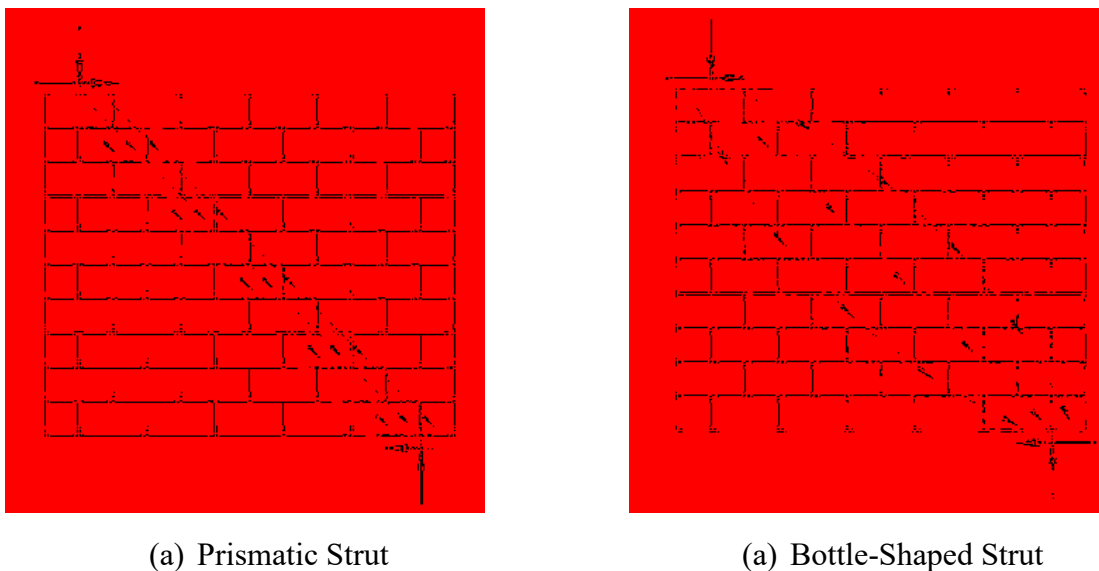
Figure 4-18: Strut Types
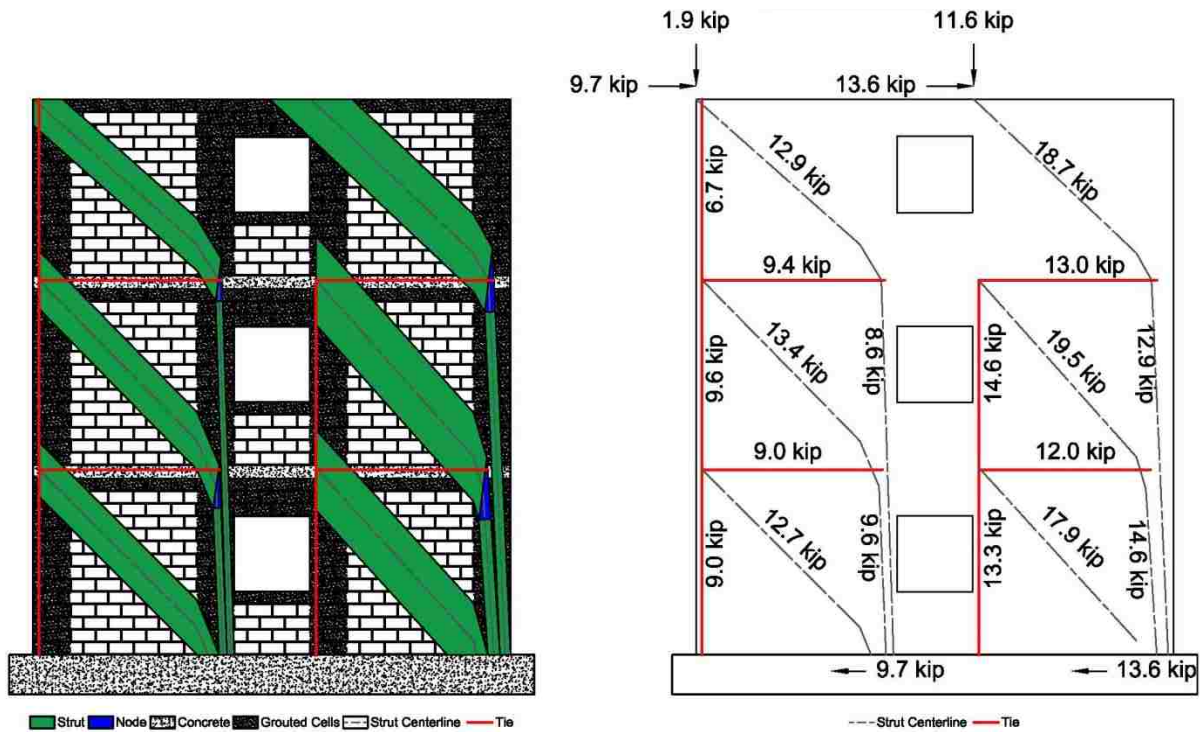
Figure 4-19: Walls 4 and 7 Strut-and-Tie Diagram

Several model were developed before arriving at the model presented herein and the strength predictions were between 7-10% less that the measured average strength. Dillon (2015) observed a similar result when analyzing the one-story high walls with doors from Voon and Ingham (2008). Dillon (2015) observed that the margin of error increased as the bottom of the opening got lower, resulting in a taller opening and a steeper strut behind the opening. The phenomenon was explained by considering the stiffnesses of the coupling beam and wall panel. In specimens with shorter openings, the shear stiffness of the panels to either side of the opening was significantly greater than that of the coupling beam. As the height of the opening increased, the aspect ratios of the panels to either side also increased, which decreased their shear stiffnesses in comparison to that of the coupling beam. The decrease in panel stiffness resulted in larger angular deformations at their tops, since they could be considered to be loaded as cantilever beams, applying a double-curvature load on the coupling beam. The loading on the

63

coupling beam produced a shear reaction in the coupling beam, which "pulls up" on the left panel and "pushes down" on the right panel. Dillon (2015) observed that the error could be mitigated by adding the shear capacity of the lintel to the tensile capacity of the tie to the right of the opening. In the model developed herein, the effect of the coupling beam was accounted for by adding the strength of a stirrup in each of the coupling beam to the total tie strength of the vertical reinforcement to the right of the opening.

5 DISCUSSION

5.1 Comparison of Analysis Methods

Table 5-1 shows the results of the various analysis methods. The upper limit imposed on the MSJC shear equation is accurate, but that model does not account for the effects of openings—it is a conservative upper bound that coincidentally is close to the measured average strength. The general MSJC shear equation and the interaction diagram are unconservative models that also do not account for wall openings. The model that used the wall panels on each side of the opening is also unconservative. There are methods for approximately distributing the shear force to wall with openings (Brandrow et al. 2015). However, those methods are not used for capacity prediction, but instead for calculating stiffnesses and subsequently lateral loads distribution.

Table 5-1: Comparison of Analysis Methods

Method	V_n [kip (kN)]	% of Average
Main MSJC Shear Equation Method 1	91 (405)	383%
Upper Limit on the MSJC Shear Equation Method 1	18.6 (82.6)	78%
Main MSJC Shear Equation Method 2	77 (343)	324%
Upper Limit on the MSJC Shear Equation Method 2	15.6 (69.6)	66%
Interaction Diagram	31.1 (138)	131%
Equivalent Truss	11.9 (52.8)	50%
Strut-and-Tie	23.6 (105)	100%

The equivalent truss model is overwhelmingly conservative with the predicted capacity being less than half of the average measured capacity. The equivalent truss model neglects the contribution of ties when calculating the width of strut and, instead, relies only upon the depth of the bond beam. The method is reasonable for predicting the strength of partially-grouted walls because it removes the iterative process that is required to determine the width of a strut in an actual strut-and-tie model. The use of a pushover analysis is advantageous because it gives not only the lateral strength of a wall, but also the displacement and the general location of failure. The displacement information is useful within seismic calculations since drift can be calculated and checked against code limits to prevent pounding between buildings. Nonetheless, the analysis has its limitations as it does not adequately describe the behavior of walls after cracking. Further research is needed for a better prediction of the post-crack response of the wall.

The strut-and-tie method provides the best modeling capabilities of any of the methods used. It is able to show the load path within the specimens as well as adequately predict the lateral strength. The strut-and-tie model also shows that the strength of a strut decreases when there is no reinforcement to limit the bottle-shaped behavior of the strut. As a result, the lateral strength decreases in walls that do not have sufficient reinforcement crossing a strut. The strut-and-tie method also shows that additional vertical load increases the lateral strength of a wall. Furthermore, the method is able to show that in multistory walls, the height of openings is irrelevant as long as a strut cannot adequately traverse beneath the opening and continue on to the edge of the wall. The reason is that struts from upper stories collect and travel downwards next to the opening. These struts do not allow other struts to traverse beneath openings because struts cannot cross each other without forming a node. Although a strut-and-tie model could be

developed with nodes under openings, such a model would be ineffective, complex, and not align to experimental observations.

The strut-and-tie method has its limitations. The method is somewhat a subjective process since nodes and struts must be laid out according to engineering judgment and an understanding of the behavior of the element being analyzed. The distribution of vertical loads is also a somewhat arbitrary process and may not be as simple as distributing according to tributary length. The greatest disadvantage of the method is that it is an iterative procedure and many iterations may be necessary to develop an optimum design, e.g., the development of the strut-and-tie model presented herein required 171 iterations. While there are computer programs available to aid in strut-and-tie modeling, these programs still require an engineer to determine location of the struts, ties, and nodes.

Strut-and-tie models also do not account for the relative stiffness of different members in a shear wall. Dillon (2015) observed that when analyzing walls with openings (Voon and Ingham, 2008), the models were under-predicting the strength of walls with door openings. The reason for the under predictions was the difference in stiffness between the panels on each side of the opening and the coupling beam above the opening. Such a shortfall can be mitigated by transferring the vertical shear force through the coupling beam across an opening to the strut on the other side of the opening. The transfer of shear forces across the openings increases the load on the strut, increases the lateral strength of the wall, and results in more accurate predictions of the wall strength. Such a modification was investigated within this study by inducing a compressive load into the tie to the right of the opening equal to the tensile capacity of a stirrup. The modification better aligned the model with the experimental results. Nonetheless, multistory, partially grouted walls have multiple elements with varying stiffnesses. Concrete, fully-grouted,

5.2 Effects of Strut-and-Tie Modifying Factors

The properties of the struts include several modifying factors to account for different phenomenon that occur within D regions. One of these factors is the strut efficiency factor, β_s. As a strut traverses between two nodes, it naturally wants to spread out to disperse energy. The dispersion results in a tensile force perpendicular to the line of compression as shown in Figure 5-1. The dispersion decreases the capacity of the strut, and to account for the dispersion, the strut efficiency factor is reduced. If a strut crosses at least one vertical or horizontal reinforcing bar, the strut efficiency factor can be increased. Reinforcement prevents the strut from fanning out similar to the way stirrups prevent shear cracks to widen. Also, if the strut is near vertical, the strut efficiency factor is 1.0 because such a struts are typically next to the edge of the wall, which prevents the compressive stress from dispersing.

Figure 5-1: Bottle-shaped Strut: (a) Cracking of a Bottle-shaped Strut; and (b) Strut-and-Tie Model of a Bottle-shaped Strut.

The strut efficiency factor was included into the strut-and-tie model developed herein and helped to account for the dispersion of compressive stresses. Even when analyzing Walls 4 and 7 with the strut efficiency factor reduced to 0.6, the predicted strength was reasonable. Thus, it appears that there is no reason to alter the values of the strut efficiency factor. More data are needed to develop and validate different values. Additional research is also needed to further investigate the effects of horizontal and vertical reinforcement and the effect of the reinforcement spacing. An analysis was also conducted with the strut efficiency factor omitted. The predicted strength for that case was 101% of the measured average strength, which is still a very reasonable result.

The nodal efficiency factor, β_n, was also incorporated into the model. The nodal efficiency factor accounts for the varying nodal configurations of which there are three: C-C-C, C-C-T, and C-T-T—C stands for compression and T stands for tension. The nodal efficiency factor is 1.0, 0.8, and 0.6 for C-C-C, C-C-T, and C-T-T nodal zones, respectively. C-C-C nodal zones are in a bi-directional state of stress. Research has shown that masonry under biaxial compression stresses demonstrates a higher effective strength than under uniaxial compression loading (Liu et al., 2006). As ties are included into the nodal zone, additional tensile stresses are induced, which lower the effectiveness of the zone due to strain incompatibility between the reinforcement and the masonry. The omission of the nodal efficiency factor in the analysis of the walls presented herein resulted in a 2.8% increase in predicted strength.

When the strut efficiency factor, β_s, and the nodal efficiency factor, β_n, are omitted in the analysis of the walls presented herein, the predicted strength is 105% of the measured average strength. Although the effect of these factors is small, their use maintains conservatism and accounts for varying phenomenon within the wall.

Dillon (2015) introduced a strut inclination factor, β_α, which was not considered in any other study. In partially-grouted walls, he theorized that increasing the strut angle would induce more shear stress into the mortar, which would lower the capacity of the strut. The strut inclination factor accounts for the decrease in strength due to the inclination angle. Dillon (2015) proposed a strut inclination factor of 1.0 for vertical strut and 0.67 for struts inclined more than 35 degrees; linear interpolation is used for inclination angles between 0 and 35 degrees. When including the β_α factor in this study, the predicted strength decreased to 95.1% of the measured average strength. Additional research is needed to either validate or refute the values proposed by Dillon (2015.)

5.3 Grouted Shear Wall Factor

The grouted shear wall factor, γ_g, was not directly investigated within this study, but the literature and calculations in this study points to its ineffectiveness. Partially-grouted walls are a complex system that exists between fully-grouted, reinforced masonry and ungrouted masonry. The possible configurations of a partially-grouted element are numerous and it would be unreasonable to expect that the same factor would account for all possible configurations. Dillon (2015) determined that the factor should be decreased from 0.75 to 0.7. While this would be more conservative, other factors should be investigated.

Nolph (2010) and Minaie et al. (2010) showed that vertical reinforcement spacing has a greater influence on shear capacity than horizontal reinforcement spacing. Nolph (2010) observed that there is no appreciable increase in capacity for horizontal reinforcement spacing less than 48 inches (for 8 in x 8 in x 16 in CMUs). He also noted that the decrease in spacing did not allow the horizontal reinforcement to reach yield. Horizontal reinforcement is necessary in

order to confine the strut and prevent it from bottling out. Vertical reinforcement is more likely to reach its yield than horizontal reinforcement because it is the tension carrying members in flexure.

Minaie et al. (2010) noted that as the spacing of horizontal reinforcement increases, the MSJC equation predicts an increase in shear capacity because it assumes that at least 50% of the reinforcement is engaged. However, such an assumption may not be always correct in which case the prediction would be unconservative. The authors remarked that the spacing of vertical grout/reinforcement appears to exert a more significant influence over the strength ratio than the spacing of horizontal spacing. The authors did not provide any explanations for this behavior, but within the context of strut-and-tie method, vertical reinforcement can act as a stirrup to confine a strut and limit shear cracking and it can also be used as a tie configured to increase the lateral strength. To account for the partial grouting condition, the authors proposed that the predicted shear strength be multiplied by the ratio of net cross-sectional area to gross cross-sectional area. The strength reduction by this ratio more closely aligned with the experimental results. The proposed approach, however, cannot be used with walls with openings as it would have the same strength reduction regardless of the opening size.

The literature and the results presented herein indicate that vertical reinforcement has a greater effect on the lateral strength of masonry shear walls than does horizontal reinforcement.

6   CONCLUSION

6.1   Summary

A study was conducted on the effect of openings and partial grouting on multistory concrete masonry shear walls. The study included the tests of six half-scale, partially grouted, multistory, masonry shear walls with either door or window openings. Walls were tested by subjecting them to a quasi-static lateral load at the top of the wall at a displacement controlled rate until failure. Samples of the different materials were also tested concurrently to the tests of the walls. The lateral strengths of the walls were measured and compared with provisions of current design codes as well as to the results of an equivalent truss analysis and a pushover analysis. In addition, a strut-and-tie model was developed and validated using the measured results.

6.2   Findings

The following conclusions can be made from the study presented herein:

1. Current MSJC design codes are unconservative and predict a significantly greater capacity than what is experimentally exhibited. The code procedure also does not account for openings. Upper limits on the code equations help to maintain some conservatism but they may lead to overly conservative results.

www.manaraa.com

2. The equivalent truss methodology as developed by Nolph (2010) and Elmapruk (2010) predicts the shear strength capacity of masonry walls reasonably well. Nonetheless, the methodology neglects the effect of tie strength and other methodologies associated with the strut-and-tie procedure.

3. Strut-and-tie modeling provides the most accurate solution for determining the lateral capacity of masonry shear walls. Strut-and-tie modeling accommodates the decreases in strength as a result of partial grouting and openings. It also explains the reason multistory walls with either door or window openings have similar results. Although iterative, the methodology gives results that are very accurate.

4. Vertical reinforcement has a greater effect on the lateral strength of masonry shear walls than does horizontal reinforcement. Horizontal reinforcement limits cracking but does not contribute significantly to the shear and flexural capacities of the wall. Vertical reinforcement can act as a stirrup to limit shear cracking and increases the shear and flexural capacities of the wall.

6.3 Recommendations for Future Research

Within the course of this study, it was observed that several other variables should be adequately tested and verified. The following topics are suggested for future research:

1. The strut efficiency factor penalizes the strength of the strut according to whether it crosses a stirrup or not. This factor should be more dynamic because it is possible that stirrups are only provided at the strut's genesis, which would still allow the strut to form a bottle-shape. Additionally, the amount of reinforcement

73

necessary to warrant an increase of the factor between 0.75 and 1.0 could be investigated.

2. Dillon (2015) proposed the inclusion of the strut inclination factor into the strut strength equation. His study showed that its inclusion into partially-grouted walls produced more accurate results. Nonetheless, its effect in this study was neglected because it did not result in a more accurate analysis. This factor should be experimentally verified to validate or invalidate the use of the strut inclination factor.

3. The strut-and-tie analysis does not allow for materials of various stiffnesses. In a partially-grouted, multistory wall, concrete, grout, mortar, and CMUs all have different stiffnesses. Although the combination of CMU, mortar, and grout can be combined into a single solid element, its stiffness would still vary whether it is partially or fully grouted. Research should be conducted to determine the effect of the stiffness of ungrouted and fully grouted portions of a partially-grouted wall.

4. A more dynamic grouted shear wall factor should be investigated to better account for varying vertical and horizontal grout/reinforcement spacings.

REFERENCES

ACI 318 (2011). *Building Code Requirements for Structural Concrete (ACI 318-02) and Commentary (ACI 318R-02).* American Concrete Institute (ACI), Farmington Hills, MI.

Balling, R. J. (2012). *Computer Structural Analysis* (Vol. 1). BYU Academic Publishing.

Brandrow, G. E., Ekwueme, C. G., and Hart G. C. (2015). *2012 Design of Reinforced Masonry Structures*, Concrete Masonry Association of California and Nevada.

Dillon, P. (2015). *Shear Strength Prediction Methods for Grouted Masonry Shear Walls.* Doctoral Dissertation, Brigham Young University, Provo, UT.

Elmapruk, J. H. (2010). *Shear Strength of Partially Grouted Squat Masonry Shear Walls.* Master's thesis, Washington State University, Pullman, WA.

Fortes, E. S. (2017). *Caracterizacão da Alvenaria Estrutural de Alta Resistência.* Ph. D. Dissertation (In Portuguese), Universidade Federal De São Carlos, São Paulo, Brazil.

Haach, V. G., Vasconcelos, G., and Lourenço, P. B. (2013). "Proposal of a Design Model for Masonry Walls Subjected to In-Plane Loading," Journal of Structural Engineering, 139, 537-547.

Klingner, R. E. and Leiva, G. (1992). "Behavior and Design of Multi-Story Masonry Walls Under In-Plane Seismic Loading." *Earthquake Engineering, Tenth World Conference*, 6, 3511.

Leiva, G., Merryman, M., Antrobus, N., and Klingner, R. E. (1990). "In-Plane Seismic Resistance of Two-Story Couple Concrete Masonry Walls." *Proceedings from the Fifth North American Masonry Conference*. University of Illinois at Urbana-Champaign.

McCormac, J. C., & Brown, R. H. (2013). Design of Reinforced Concrete, 9th Edition (9th ed.). John Wiley & Sons.

75

Minaie, E., Mota, M., Moon, F. L., and Hamid, A. A. (2010). "In-Plane Behavior of Partially Grouted Reinforced Concrete Shear Walls." Journal of Structural Engineering 136(9), 1089-1097.

MSJC (2013). Building Code Requirements for Masonry Structures (TMS 402–13, ACI 530–13, and ASCE 5–13). The Masonry Society, American Concrete Institute, and ASCE, Boulder, CO; Farmington Hills, MI; and Reston, VA.

Nolph, S. M. (2010). *In–Plane Shear Performance of Partially Grouted Masonry Shear Walls*. Master's thesis, Washington State University, Pullman, WA.

Nolph, S. M. and ElGawady, M. A. (2012). "Static cyclic response of partially grouted masonry shear walls." Journal of Structural Engineering, 138(7), 864– 879.

Schlaich, J., Schäfer, K., and Jennewein, M. (1987). "Toward a consistent design of structural concrete." Journal of the Prestressed Concrete Institute, 32(3), 74–150.

Voon, K. C. and Ingham, J. M. (2006). "Experimental in-plane shear strength investigation of reinforced concrete masonry walls." Journal of Structural Engineering, 132(3), 400–408.

Voon, K. C. and Ingham, J. M. (2008). "Experimental in-plane investigation of reinforced concrete masonry walls with openings." Journal of Structural Engineering, 134(5), 758– 768.
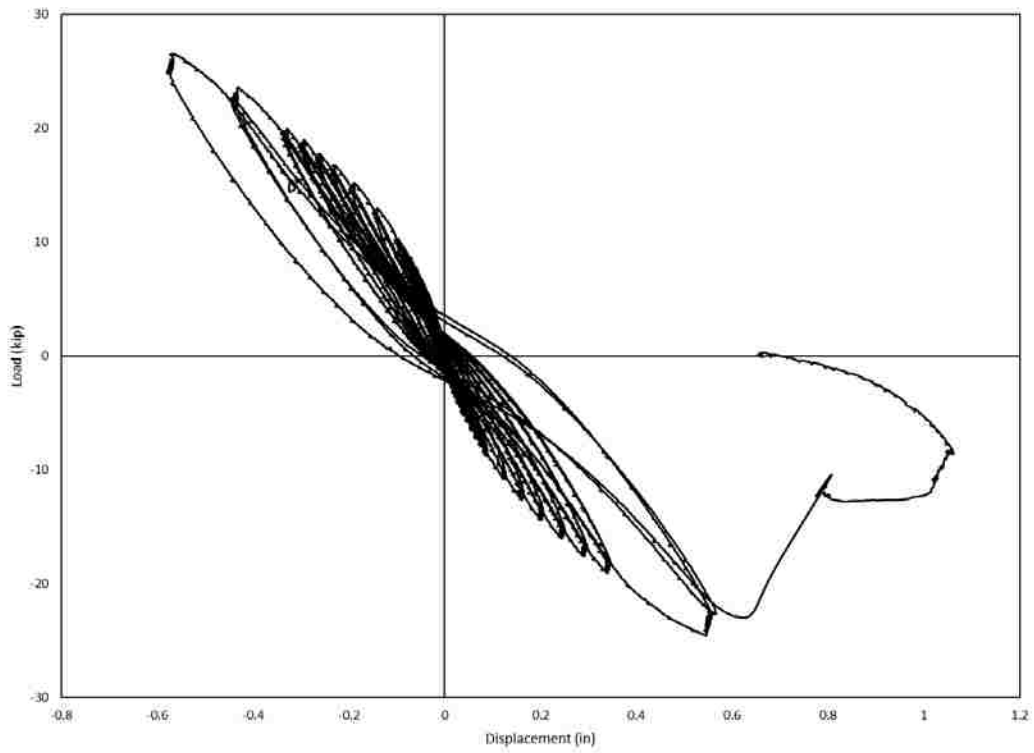
APPENDIX A.   LOAD-DISPLACEMENT CURVES

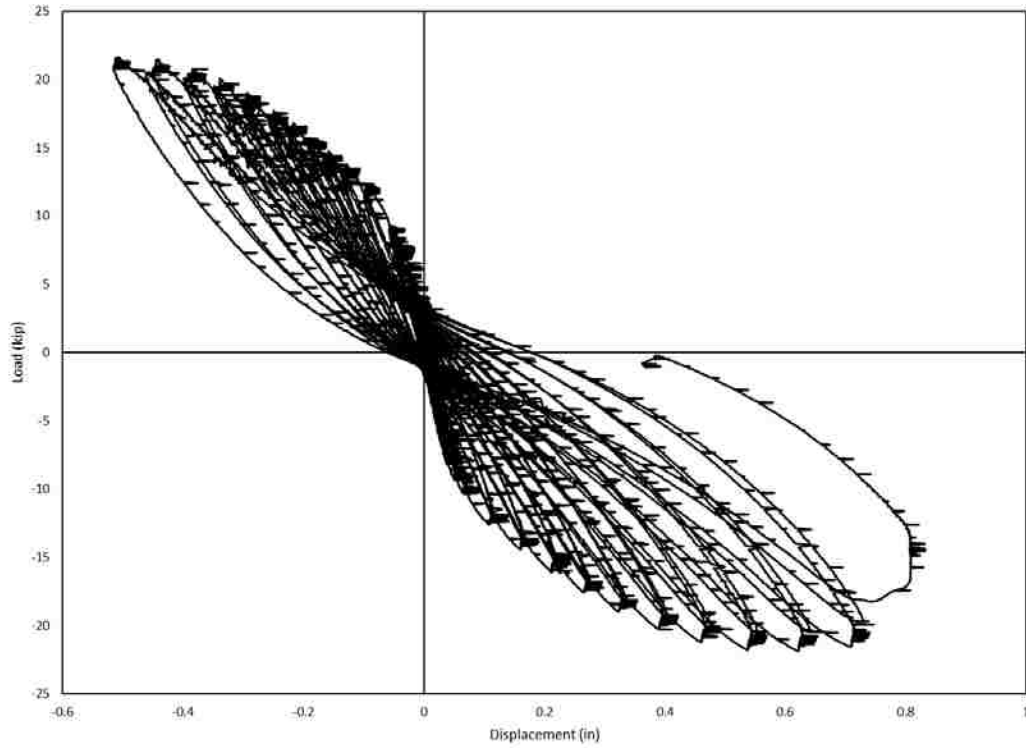Figure A-1: Wall 1 Load-Displacement Diagram
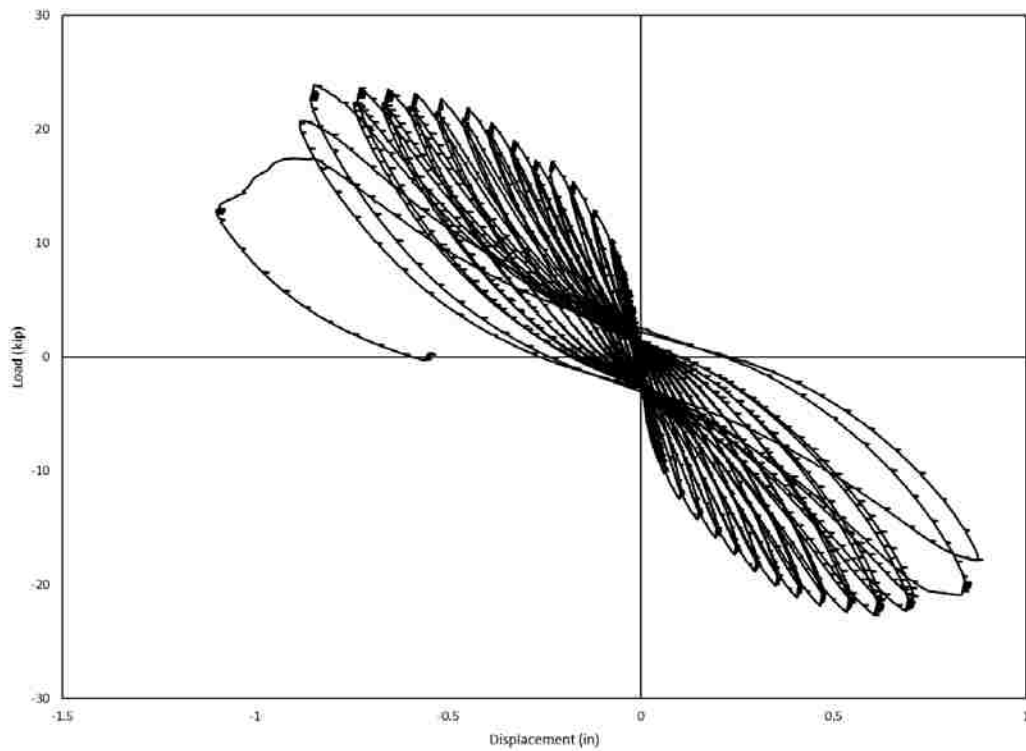
Figure A-2: Wall 5 Load-Displacement Diagram

Figure A-3: Wall 8 Load-Displacement Diagram
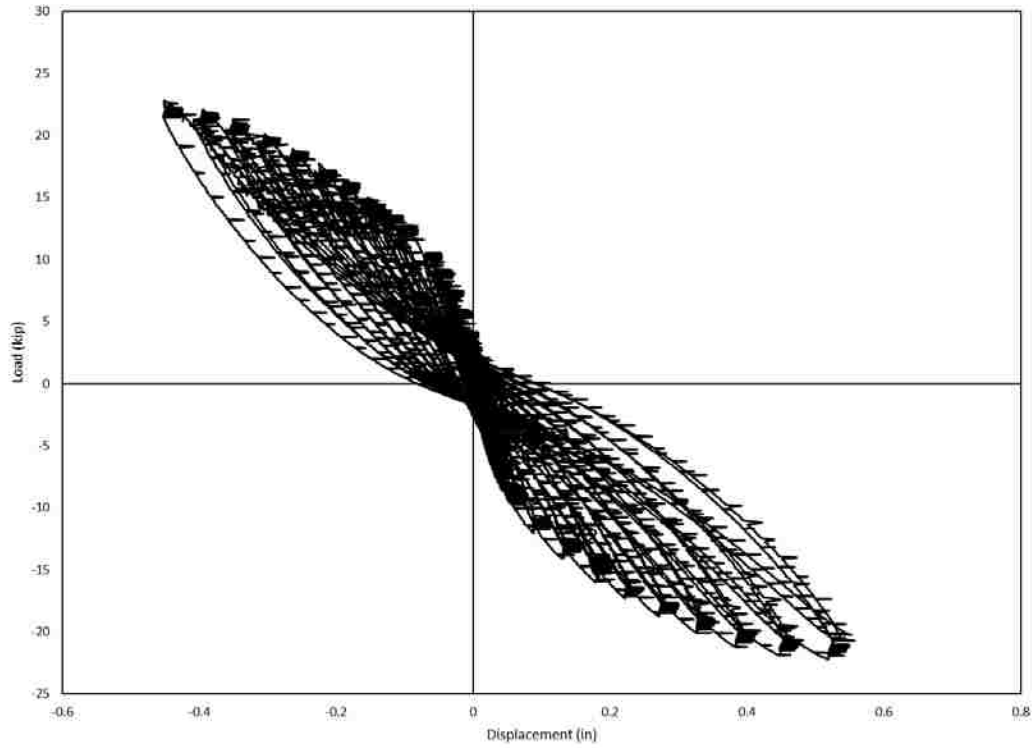
78

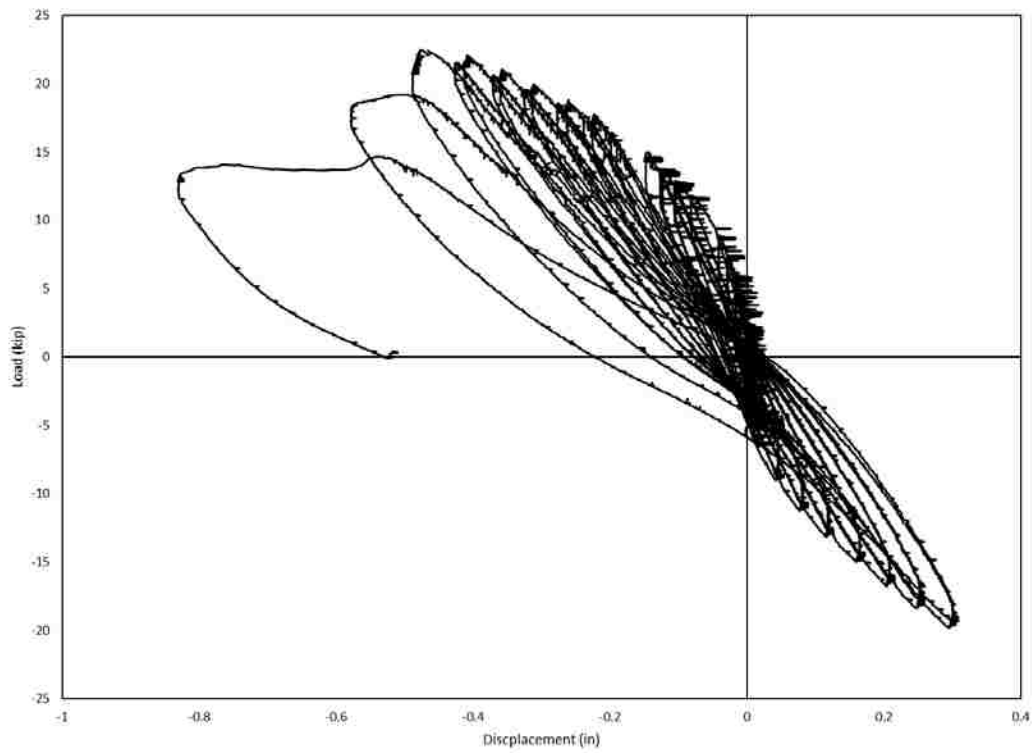Figure A-4: Wall 4 Load-Displacement Diagram

Figure A-5: Wall 7 Load-Displacement Diagram
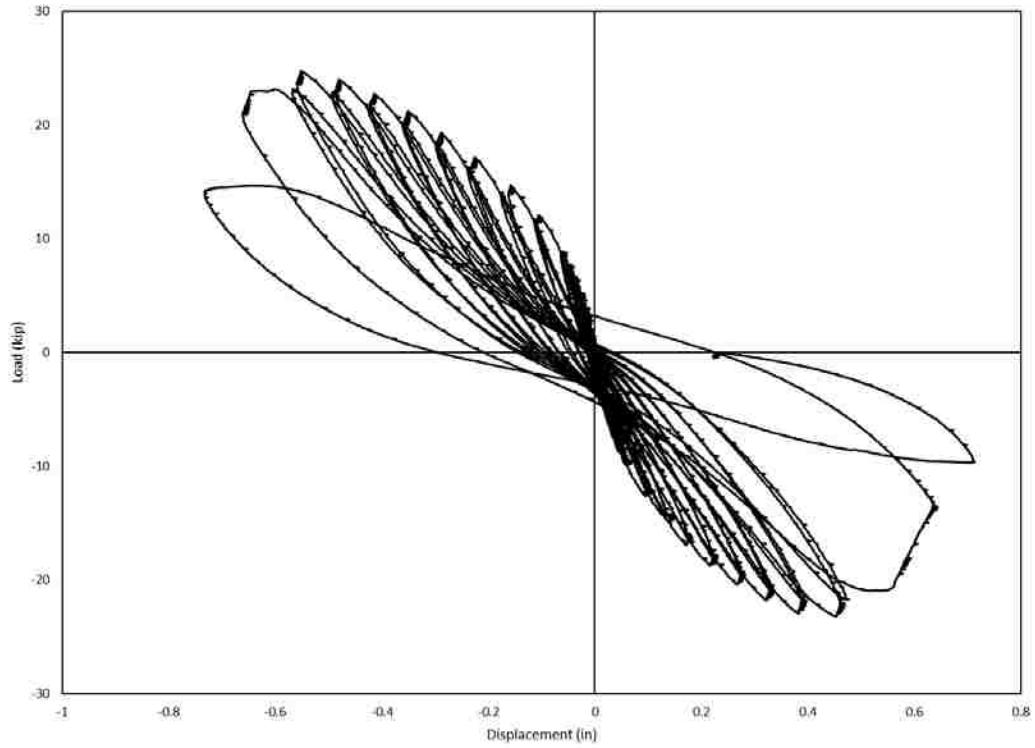
Figure A-6: Wall 10 Load-Displacement Diagram

APPENDIX B.   SAMPLE TESTING

Concrete, mortar, grout, CMU block and masonry prism samples were prepared throughout the project and were tested immediately following the lateral shear wall test. The samples were tested in general accordance with the protocols outlined in the American Society for Testing and Materials (ASTM) C109 (Standard Test Method for Compressive Strength of Hydraulic Cement Mortars (Using 2-in. or [50-mm] Cube Specimens)), ASTM C1019 (Standard Test Method for Sampling and Testing Grout), ASTM C1314 (Standard Test Method for Compressive Strength of Masonry Prisms), ASTM C1552 (Standard Practice for Capping Concrete Masonry Units, Related Units and Masonry Prisms for Compression Testing), ASTM C617 (Standard Practice for Capping Cylindrical Concrete Specimens), ASTM C39 (Standard Test Method for Compressive Strength of Cylindrical Concrete Specimens), and ASTM C140 (Standard Methods for Sampling and Testing Concrete Masonry Units and Related Units) as shown in Figure B-1 through Figure B-5. Maximum compression loads were documented and for some grout prisms and CMU prisms, string pots were used in order to calculate their modulus of elasticity as shown in Figure B-2 and Figure B-5. The average values for the samples for all walls is summarized in Table B-1.

Table B-1. Component Data for all Walls (psi)

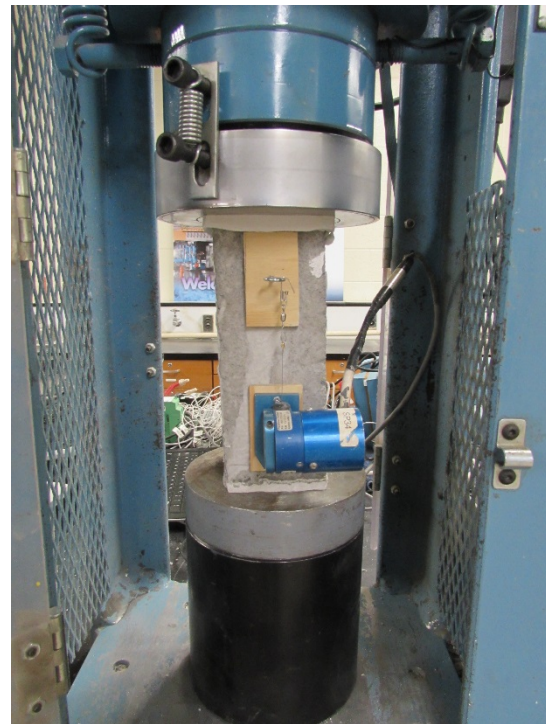| Wall	Mortar	Concrete	Grout	CMU gross	CMU Net	Hallow Prism	Grouted Prism
1	-	-	4413	-	-	-	-
2	2912	5293	-	-	-	-	1454
3	2154	5001	5817	-	-	1168	1469
4	2277	4812	4866	-	-	1803	2140
5	2465	4514	5199	1460	2869	-	-
6	2192	5204	4264	1818	3572	-	-
7	2115	4552	4625	933	1832	-	-
8	2104	4848	4525	-	-	-	-
9	-	5307	6717	1286	2527	-	-
10	1844	5158	6996	1346	2644	-	-
Average	2258	4965	5269	1369	2689	1486	1688

Figure B-1: Capping CMU Blocks

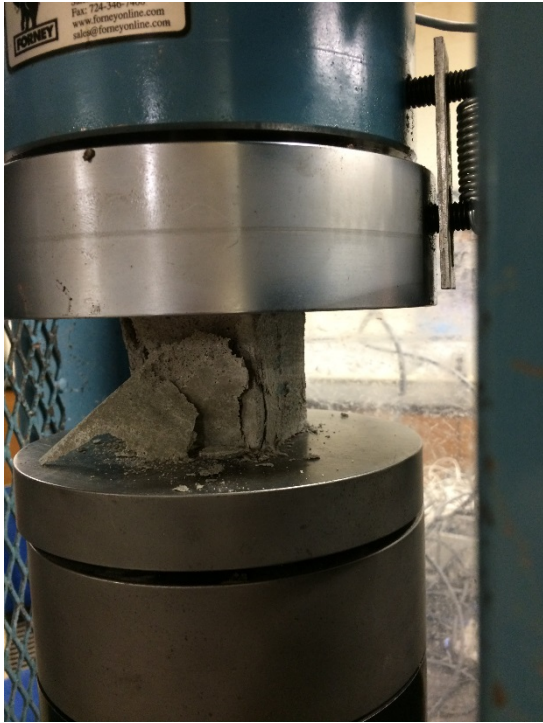Figure B-2: Testing of Grout Prism Sample using a String Pot

82

Figure B-3: Testing of Mortar Cube

Figure B-4: Testing of Concrete Cylinder

Figure B-5: Testing of CMU Prism using String Pots

APPENDIX C.   MSJC SHEAR EQUATION CALCULATIONS

Method 1:

Constants:

$h_w := 4.19m = 13.75\ ft$ $d_v := 3.6m = 11.81\ ft$ $\gamma_g := 0.75$ $\phi := 0.8$ $t_{sh} := .643in$

$P := 13.43kip$ $f_m := 1803psi$ $no_{bar} := 6$ $f_y := 76.59ksi$

Contribution from Masonry:

$$ratio := \min\left(\frac{h_w}{d_v}, 1\right) = 1$$

$$A_{nv} := 2 \cdot t_{sh} \cdot d_v = 182.27 \cdot in^2$$

$$P_u := 1.2 \cdot P = 16.12 \cdot kip$$

$$V_{nm} := \left[(4 - 1.75) \cdot ratio \cdot A_{nv} \sqrt{f_m \cdot psi} + .25 \cdot P_u\right] = 21.44\ kip$$

Contribution from Steel:

$$A_s := no_{bar} \cdot 0.11in^2 = 0.66 \cdot in^2$$

$$s := \frac{h_w}{no_{bar}} = 27.49 \cdot in$$

$$\rho_{ht} := \frac{A_s}{s} = 2 \times 10^{-3} ft$$

$$V_{ns} := .5 \cdot \rho_{ht} \cdot f_y \cdot d_v = 130.29 \cdot kip$$

$$V_n := (V_{nm} + V_{ns}) \cdot \gamma_g = 113.8 \cdot kip$$

$$\phi V_n := \phi \cdot V_n = 91.04\ kip$$

$$\phi V_{n\_max} := \phi \cdot 4 \cdot A_{nv} \sqrt{f_m \cdot psi} \cdot \gamma_g = 18.57 \cdot kip$$

Method 2:

Constants:

$$h_w := 4.19m = 13.75 \, ft \qquad d_v := 1.515m = 4.97 \, ft \qquad \gamma_g := 0.75 \qquad \phi := 0.8 \qquad t_{sh} := .643in$$

$$P := \frac{13.43kip}{2} \qquad f_m := 1803psi \qquad no_{bar} := 6 \qquad f_y := 76.59ksi$$

Contribution from Masonry:

$$ratio := min\left(\frac{h_w}{d_v}, 1\right) = 1$$

$$A_{nv} := 2 \cdot t_{sh} \cdot d_v = 76.7 \cdot in^2$$

$$P_u := 1.2 \cdot P = 8.06 \, kip$$

$$V_{nm} := \left[(4 - 1.75) \cdot ratio \cdot A_{nv} \sqrt{f_m \cdot psi} + .25 \cdot P_u\right] = 9.34 \, kip$$

Contribution from Steel:

$$A_s := no_{bar} \cdot 0.11in^2 = 0.66 \cdot in^2$$

$$s := \frac{h_w}{no_{bar}} = 27.49 \cdot in$$

$$\rho_{ht} := \frac{A_s}{s} = 2 \times 10^{-3} \, ft$$

$$V_{ns} := .5 \, \rho_{ht} \cdot f_y \cdot d_v = 54.83 \, kip$$

$$V_n := (V_{nm} + V_{ns}) \cdot \gamma_g = 48.13 \, kip$$

$$\phi V_n := \phi \cdot V_n = 38.5 \, kip$$

$$\phi V_{n\_total} := 2 \cdot \phi V_n = 77.01 \, kip$$

$$\phi V_{n\_max} := \phi \cdot 4 \cdot A_{nv} \sqrt{f_m \cdot psi} \cdot \gamma_g = 7.82 \, kip$$

$$V_{n\_max\_total} := 2 \cdot \phi V_{n\_max} = 15.63 \, kip$$

APPENDIX D.   PUSHOVER ANALYSIS INPUTS

Table D-1: Joint Coordinates

num	x	y
1	0	0
2	47.73622	0
3	82.97244	0
4	130.7087	0
5	0	56.29921
6	47.73622	56.29921
7	82.97244	56.29921
8	130.7087	56.29921
9	0	112.5984
10	47.73622	112.5984
11	82.97244	112.5984
12	130.7087	112.5984
13	0	168.8976
14	47.73622	168.8976
15	82.97244	168.8976
16	130.7087	168.8976

Table D-2: Supports

num	joint	direction
1	1	1
2	1	2
3	2	1
4	2	2
5	3	1
6	3	2
7	4	1
8	4	2

Table D-3: Member Data

num	joint 1	joint 2	section
1	1	5	1
2	5	6	3
3	2	6	2
4	2	5	4
5	6	7	3
6	3	7	1
7	7	8	3
8	4	8	2
9	4	7	4
10	5	9	1
11	9	10	3
12	6	10	2
13	6	9	4
14	10	11	3
15	7	11	1
16	11	12	3
17	8	12	2
18	8	11	4
19	9	13	1
20	13	14	6
21	10	14	2
22	10	13	8
23	14	15	7
24	11	15	1
25	15	16	6
26	12	16	2
27	12	15	8

Table D-4: Material and Section Properties

num	type	E	A	I	E1	E2	RIBUCK	RF	RM	RV
1	3 #3 rebar	29000	0.33	3.244	1	1	0.004	0.040	0.005	0.076
2	Column	3627	39.13	41.10	1	1	0.024	0.013	0.007	0.476
3	Beam (tie)	29000	0.22	1.262	1	1	0.000	0.059	0.013	0.076
4	Strut Story 1 and 2	2455	13.25	144.8	0	0	0.000	0.082	0.033	2.765
5	Beam (comp)	4170	64.35	215.8	1	1	0.002	0.003	0.002	0.088
6	Top Beam	3790	169.00	2380	1	1	0.000	0.001	0.001	0.056
7	Top Lintel	3724	208.13	7361	1	1	0.000	0.001	0.000	0.049
8	Strut Story 3	2455	17.53	307.2	0	0	0.000	0.079	0.022	2.361

Table D-5: Joint Loads

num	joint	direction	magnitude
1	13	2	-2.24
2	14	2	-4.48
3	15	2	-4.48
4	16	2	-2.24

Table D-6: Nonlinear Pushover Inputs

number of pushover levels	1000000
iteration convergence tolerance	0.001
maximum number of iterations	1000
number of iterations with same stiffness	1
number of pushover loads	1
number of plotted displacements	1

Table D-7: Pushover Loads

num	joint	direction	magnitude
1	13	1	0.01

APPENDIX E.   STRUT-AND-TIE CALCULATIONS

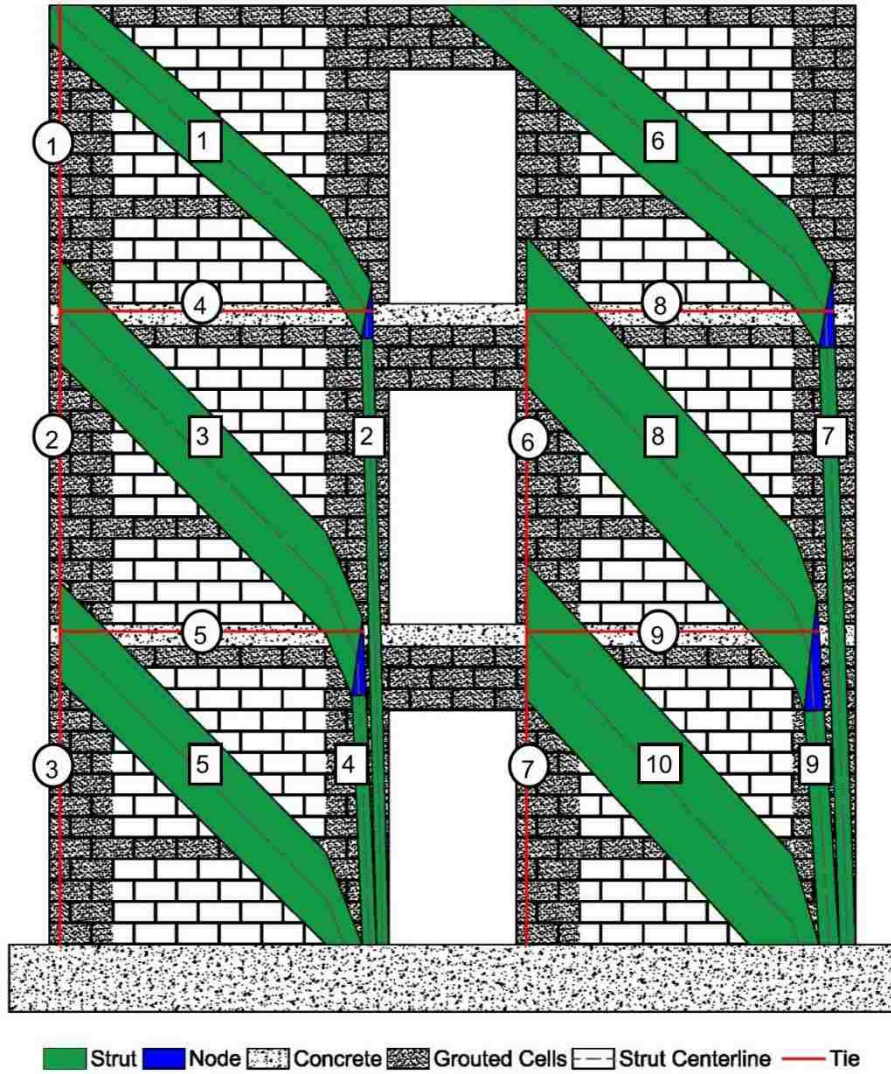For the following calculations, refer to Figure E-1.

Figure E-1: Labeled Strut-and-Tie Diagram

Table E-1: Strut-and-Tie Calculations for Initial Conditions

Left-side of Wall				
	P_1		3.17	kip
	F_{1y}		0.02	kip
	T_{total}		6.86	kip
	Ties	1	0.02	kip
		2	3.48	kip
		3	3.36	kip
		4	3.97	kip
		5	3.91	kip
	V_1		4.00	kip

Right-side of Wall				
	P_2		10.27	kip
	F_{2y}		0.00	kip
	T_{total}		28.10	kip
	Ties	6	15.68	kip
		7	12.42	kip
		8	17.06	kip
		9	14.45	kip
	V_2		17.80	kip
	V_{total}		21.80	kip

Strut	β_n	β_s	x (in)	y (in)	a_0 (in)	α	F_y (kip)	F_x (kip)	F_s (kip)	w (in)	a_1 (in)	$a_1 - a_0$ (in)
1	1.00	0.75	71.26	53.68	3.94	51.43	3.19	4.00	5.12	3.67	5.89	1.96
2	0.80	1.00	1.97	111.28	0.79	0.61	3.19	0.03	3.19	0.78	0.78	-0.01
3	0.60	0.75	68.12	56.30	3.94	48.74	3.48	3.97	5.28	4.74	7.18	3.24
4	0.80	1.00	1.66	54.98	0.79	0.91	3.48	0.06	3.48	0.85	0.85	0.06
5	0.60	0.75	67.91	54.98	3.94	49.32	3.36	3.91	5.16	4.63	7.10	3.17
6	1.00	0.75	86.56	53.68	3.94	56.99	11.56	17.80	21.22	15.24	27.97	24.04
7	0.80	1.00	7.85	111.28	0.79	3.63	11.56	0.73	11.59	2.83	2.84	2.05
8	0.60	0.75	65.21	56.30	3.94	47.42	15.68	17.06	23.17	20.80	30.74	26.80
9	0.80	1.00	9.94	54.98	0.79	9.45	15.68	2.61	15.89	3.89	3.94	3.15
10	0.60	0.75	67.91	54.98	3.94	49.32	12.42	14.45	19.06	17.10	26.24	22.30

Table E-2: Strut-and-Tie Calculations after the 19th Iteration

Left-side of Wall	P_1		3.71	kip
	F_{1y}		0.02	kip
	T_{total}		8.00	kip
	Ties	1	0.02	kip
		2	4.08	kip
		3	3.91	kip
		4	4.64	kip
		5	4.55	kip
	V_1		4.69	kip
Right-side of Wall	P_2		9.73	kip
	F_{2y}		0.00	kip
	T_{total}		26.64	kip
	Ties	6	13.84	kip
		7	12.80	kip
		8	12.68	kip
		9	11.82	kip
	V_2		13.05	kip
	V_{total}		17.73	kip

Strut	β_n	β_s	x (in)	y (in)	a_0 (in)	α	F_y (kip)	F_x (kip)	F_s (kip)	w (in)	a_1 (in)	a_1-a_0 (in)
1	1.00	0.75	71.26	53.68	3.94	51.43	3.74	4.69	5.99	4.30	6.90	2.96
2	0.80	1.00	2.23	111.28	0.79	0.74	3.74	0.05	3.74	0.91	0.91	0.13
3	0.60	0.75	67.98	56.30	3.94	48.68	4.08	4.64	6.17	5.54	8.39	4.46
4	0.80	1.00	2.02	54.98	0.79	1.28	4.08	0.09	4.08	1.00	1.00	0.21
5	0.60	0.75	67.91	54.98	3.94	49.32	3.91	4.55	5.99	5.38	8.25	4.32
6	1.00	0.75	82.58	53.68	19.01	49.82	11.02	13.05	17.08	12.26	19.00	0.00
7	0.80	1.00	6.42	111.28	2.70	1.91	11.02	0.37	11.02	2.70	2.70	0.00
8	0.60	0.75	74.41	56.30	22.85	42.48	13.84	12.68	18.77	16.85	22.85	0.00
9	0.80	1.00	6.81	54.98	3.40	3.55	13.84	0.86	13.87	3.39	3.40	0.00
10	0.60	0.75	72.06	54.98	21.28	42.72	12.80	11.82	17.42	15.64	21.29	0.00

Table E-3: Strut-and-Tie Calculations after the 32nd Iteration

				Value	Unit
Left-side of Wall		P_1		3.29	kip
		F_{1y}		0.02	kip
		T_{total}		7.12	kip
	Ties		1	0.02	kip
			2	4.08	kip
			3	3.91	kip
			4	4.64	kip
			5	4.55	kip
		V_1		4.16	kip
Right-side of Wall		P_2		10.15	kip
		F_{2y}		0.00	kip
		T_{total}		27.57	kip
	Ties		6	14.35	kip
			7	13.23	kip
			8	13.02	kip
			9	12.10	kip
		V_2		13.41	kip
		V_{total}		17.57	kip

Strut	β_n	β_s	x (in)	y (in)	a_0 (in)	α	F_y (kip)	F_x (kip)	F_s (kip)	w (in)	a_1 (in)	a_1-a_0 (in)
1	1.00	0.75	71.26	53.68	3.94	51.43	3.31	4.16	5.32	3.82	6.12	2.19
2	0.80	1.00	2.03	111.28	0.79	0.64	3.31	0.04	3.31	0.81	0.81	0.02
3	0.60	0.75	68.09	56.30	3.94	48.73	3.62	4.12	5.48	4.92	7.46	3.52
4	0.80	1.00	1.74	54.98	0.79	0.99	3.62	0.06	3.62	0.88	0.88	0.10
5	0.60	0.75	67.91	54.98	3.94	49.32	3.49	4.06	5.35	4.80	7.37	3.43
6	1.00	0.75	82.45	53.68	19.51	49.54	11.44	13.41	17.63	12.66	19.50	0.00
7	0.80	1.00	6.60	111.28	2.80	1.96	11.44	0.39	11.44	2.80	2.80	0.00
8	0.60	0.75	74.58	56.30	23.48	42.23	14.35	13.02	19.37	17.39	23.48	0.00
9	0.80	1.00	7.06	54.98	3.52	3.68	14.35	0.92	14.38	3.52	3.52	0.00
10	0.60	0.75	72.10	54.98	21.80	42.45	13.23	12.10	17.93	16.09	21.81	0.00

Table E-4: Strut-and-Tie Calculations after the 50th Iteration

	P_1		3.17	kip
	F_{1y}		0.02	kip
Left-side of Wall	T_{total}		6.86	kip
	Ties	1	0.02	kip
		2	4.08	kip
		3	3.91	kip
		4	4.64	kip
		5	4.55	kip
	V_1		4.00	kip
	P_2		10.27	kip
	F_{2y}		0.00	kip
Right-side of Wall	T_{total}		27.85	kip
	Ties	6	14.50	kip
		7	13.35	kip
		8	13.12	kip
		9	12.18	kip
	V_2		13.52	kip
	V_{total}		17.52	kip

Strut	β_n	β_s	x (in)	y (in)	a_0 (in)	α	F_y (kip)	F_x (kip)	F_s (kip)	w (in)	a_1 (in)	$a_1 - a_0$ (in)
1	1.00	0.75	71.26	53.68	3.94	51.43	3.19	4.00	5.11	3.67	5.89	1.95
2	0.80	1.00	1.96	111.28	0.79	0.61	3.19	0.03	3.19	0.78	0.78	-0.01
3	0.60	0.75	68.12	56.30	3.94	48.74	3.48	3.97	5.28	4.73	7.18	3.24
4	0.80	1.00	1.66	54.98	0.79	0.91	3.48	0.06	3.48	0.85	0.85	0.06
5	0.60	0.75	67.91	54.98	3.94	49.32	3.36	3.91	5.16	4.63	7.10	3.16
6	1.00	0.75	82.41	53.68	19.65	49.46	11.56	13.52	17.79	12.77	19.65	0.00
7	0.80	1.00	6.66	111.28	2.83	1.97	11.56	0.40	11.57	2.83	2.83	0.00
8	0.60	0.75	74.63	56.30	23.67	42.15	14.50	13.12	19.55	17.55	23.67	0.00
9	1.00	0.75	71.26	53.68	3.94	51.43	3.19	4.00	5.11	3.67	5.89	1.95
10	0.80	1.00	1.96	111.28	0.79	0.61	3.19	0.03	3.19	0.78	0.78	-0.01

			Value	Unit
Left-side of Wall	P_1		3.17	kip
	F_{1y}		0.02	kip
	T_{total}		6.94	kip
	Ties	1	0.02	kip
		2	4.08	kip
		3	3.91	kip
		4	4.64	kip
		5	4.55	kip
	V_1		3.94	kip
Right-side of Wall	P_2		10.27	kip
	F_{2y}		0.00	kip
	T_{total}		27.85	kip
	Ties	6	14.50	kip
		7	13.35	kip
		8	13.12	kip
		9	12.18	kip
	V_2		13.52	kip
	V_{total}		17.46	kip

Strut	β_n	β_s	x (in)	y (in)	a_0 (in)	α	F_y (kip)	F_x (kip)	F_s (kip)	w (in)	a_1 (in)	a_1-a_0 (in)
1	1.00	0.75	72.19	53.68	5.79	51.05	3.19	3.94	5.07	3.64	5.79	0.00
2	0.80	1.00	1.93	111.28	0.78	0.59	3.19	0.03	3.19	0.78	0.78	0.00
3	0.60	0.75	69.70	56.30	7.06	48.05	3.52	3.91	5.26	4.72	7.06	0.00
4	0.80	1.00	1.66	54.98	0.86	0.84	3.52	0.05	3.52	0.86	0.86	0.00
5	0.60	0.75	69.37	54.98	6.98	48.61	3.40	3.86	5.14	4.62	6.98	0.00
6	1.00	0.75	82.41	53.68	19.65	49.46	11.56	13.52	17.79	12.77	19.65	0.00
7	0.80	1.00	6.66	111.28	2.83	1.97	11.56	0.40	11.57	2.83	2.83	0.00
8	0.60	0.75	74.63	56.30	23.67	42.15	14.50	13.12	19.55	17.55	23.67	0.00
9	0.80	1.00	7.13	54.98	3.56	3.72	14.50	0.94	14.53	3.55	3.56	0.00
10	0.60	0.75	72.11	54.98	21.96	42.37	13.35	12.18	18.07	16.22	21.96	0.00

Table E-6: Strut-and-Tie Calculations after the 64th Iteration

			Value	Unit
Left-side of Wall	P_1		3.17	kip
	F_{1y}		0.04	kip
	T_{total}		6.99	kip
	Ties	1	0.02	kip
		2	4.08	kip
		3	3.91	kip
		4	4.64	kip
		5	4.55	kip
	V_1		3.96	kip
Right-side of Wall	P_2		10.27	kip
	F_{2y}		0.00	kip
	T_{total}		27.85	kip
	Ties	6	14.50	kip
		7	13.35	kip
		8	13.12	kip
		9	12.18	kip
	V_2		13.52	kip
	V_{total}		17.48	kip

Strut	β_n	β_s	x (in)	y (in)	a_0 (in)	α	F_y (kip)	F_x (kip)	F_s (kip)	w (in)	a_1 (in)	a_1-a_0 (in)
1	1.00	0.75	72.20	53.68	5.82	51.04	3.21	3.96	5.10	3.66	5.82	0.00
2	0.80	1.00	1.94	111.28	0.78	0.60	3.21	0.03	3.21	0.78	0.78	0.00
3	0.60	0.75	69.71	56.30	7.09	48.04	3.53	3.93	5.29	4.74	7.09	0.00
4	0.80	1.00	1.67	54.98	0.86	0.84	3.53	0.05	3.53	0.86	0.86	0.00
5	0.60	0.75	69.38	54.98	7.02	48.60	3.42	3.88	5.17	4.64	7.02	0.00
6	1.00	0.75	82.41	53.68	19.65	49.46	11.56	13.52	17.79	12.77	19.65	0.00
7	0.80	1.00	6.66	111.28	2.83	1.97	11.56	0.40	11.57	2.83	2.83	0.00
8	0.60	0.75	74.63	56.30	23.67	42.15	14.50	13.12	19.55	17.55	23.67	0.00
9	0.80	1.00	7.13	54.98	3.56	3.72	14.50	0.94	14.53	3.55	3.56	0.00
10	0.60	0.75	72.11	54.98	21.96	42.37	13.35	12.18	18.07	16.22	21.96	0.00

Table E-7: Strut-and-Tie Calculations after the 171st Iteration

	P$_1$		3.17	kip
Left-side of Wall	F$_{1y}$		5.60	kip
	T$_{total}$		25.27	kip
	Ties	1	5.60	kip
		2	10.11	kip
		3	9.56	kip
		4	9.89	kip
		5	9.46	kip
	V$_1$		10.12	kip
Right-side of Wall	P$_2$		10.27	kip
	F$_{2y}$		0.00	kip
	T$_{total}$		27.85	kip
	Ties	6	14.50	kip
		7	13.35	kip
		8	13.12	kip
		9	12.18	kip
	V$_2$		13.52	kip
	V$_{total}$		23.64	kip

Strut	β$_n$	β$_s$	x (in)	y (in)	a$_0$ (in)	α	F$_y$ (kip)	F$_x$ (kip)	F$_s$ (kip)	w (in)	a$_1$ (in)	a$_1$-a$_0$ (in)
1	1.00	0.75	76.63	53.68	14.68	49.09	8.77	10.12	13.39	9.61	14.68	0.00
2	0.80	1.00	4.99	111.28	2.14	1.46	8.77	0.22	8.77	2.14	2.15	0.00
3	0.60	0.75	72.85	56.30	17.76	44.38	10.11	9.89	14.15	12.70	17.76	0.00
4	0.80	1.00	4.81	54.98	2.48	2.43	10.11	0.43	10.12	2.47	2.48	0.00
5	0.60	0.75	71.39	54.98	16.99	44.70	9.56	9.46	13.45	12.08	16.99	0.00
6	1.00	0.75	82.41	53.68	19.65	49.46	11.56	13.52	17.79	12.77	19.65	0.00
7	0.80	1.00	6.66	111.28	2.83	1.97	11.56	0.40	11.57	2.83	2.83	0.00
8	0.60	0.75	74.63	56.30	23.67	42.15	14.50	13.12	19.55	17.55	23.67	0.00
9	0.80	1.00	7.13	54.98	3.56	3.72	14.50	0.94	14.53	3.55	3.56	0.00
10	0.60	0.75	72.11	54.98	21.96	42.37	13.35	12.18	18.07	16.22	21.96	0.00